Proc. of SPIE Vol. 2743, Infrared Imaging Systems: Design, Analysis, Modeling, and Testing VII, ed. G C Holst (Jun 1996) Copyright SPIE

Methodology for Rapid Infrared Multi-Spectral, Electro-Optical Imaging System Performance Analysis and Synthesis

Bradly J. Cooke, Bryan E. Laubscher and Christoph C. Borel

Los Alamos National Laboratory
MS - D448, P.O. Box 1663
Los Alamos, New Mexico 87545

Terrence S. Lomheim and Christopher F. Klein

The Aerospace Corporation
MS -M4-980, P.O. Box 92957
Los Angeles, California 90009-2957

ABSTRACT

An analysis methodology and corresponding analytical tools for rapid top-down design of multi-spectral imaging systems is presented. Beginning with top-level customer-dictated system performance requirements and constraints, the critical system and component parameters in the electro-optical image chain are derived, performance analyzed, and iterated until a preliminary design that meets customer requirements is generated. System parameters and components composing the image chain for staring, scanning, pushbroom, and time-delay and integrate (TDI) systems include: aperture, focal length, field of view, cold shield requirements, image plane dimensions, pixel dimensions, pixel pitch and fill factor, detection quantum efficiency, optical filter requirements, and temporal sampling parameters. The performance analysis is accomplished by calculating the imaging system's optical response (to a scene radiance), total noise, and imaging resolution. The noise components include photon noise due to signal, scene and atmospheric background, cold shield, out-of-band optical filter leakage and electronic noise. System resolution is simulated through cascaded optical transfer functions (OTF's) and includes effects due to atmosphere, optics, image sampling, and system motion.

Keywords: multi-spectral imager, electro-optical imaging, design synthesis, performance analysis

1. INTRODUCTION

It is the purpose of this paper to provide practical analysis tools that will rapidly lead to a preliminary electro-optical design based on a top-level definition of system requirements. Once the basic image chain elements, including optics, focal plane array and electronics have been specified, the system can then be partitioned and procured as individual subsystems. In this manner, a timely, optimized, cost effective electro-optical imaging system can be designed with system parameters and specifications driven by customer top-level requirements.

1.1. Electro-optical infrared imaging system

The basic function of an infrared (IR) electro-optical imaging system is the optical collection, electro-optical conversion, electronic processing and multiplexing, digital data transmission, image reconstruction, and display of object plane image information created by radiation and reflected IR electromagnetic energy. The major functions associated with a typical electro-optical image chain are shown in **Figure 1**. IR radiation from a target image propagates through the atmosphere, and is mapped onto an image plane through collection optics, then sampled, and converted into electronic signals for transmission, data processing and display. The actual configuration and implementation of a given image chain depends strongly on the top-level requirements and resulting flow-down system specifications. For what immediately

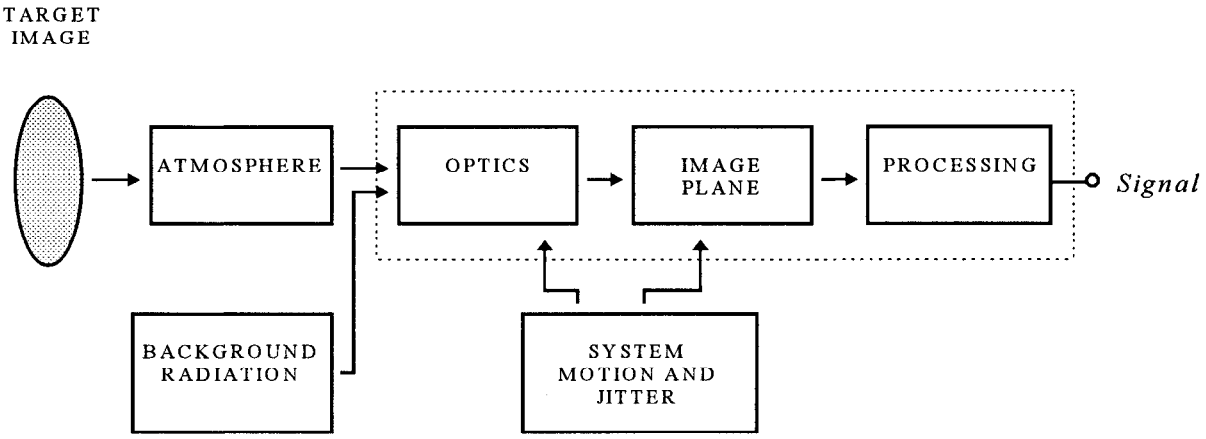

Figure 1. Electro-Optical Imaging System

follows and throughout the remainder of this paper, *Signal*, will always represent the desired physical measurement with the effectiveness of the measurement given by the signal-to-noise ratio (SNR)[1]

$$SNR = \frac{Signal}{\sigma_{system}} \quad , \tag{1}$$

where *Signal* is the mean signal value and σ_{system} is the signal standard deviation due to system noise. The composition of system noise and how it is calculated is addressed later in the paper.

1.2. The first step in electro-optical system design: defining performance and synthesis requirements

The best way to initiate a robust system design is by first scripting a precise statement of the performance requirements followed by a concise system synthesis prescription that clearly relates performance requirements to synthesis requirements. The design methodology for a complex electro-optical imaging system should be no less robust – a clear definition of the performance requirements and synthesis requirements is an essential first step in the design process. As will be elaborated below, electro-optical imaging systems performance requirements are derived from top-level, customer-directed specifications, while synthesis requirements come in to play during the flow-down process of translating performance requirements into realizable system specifications (read hardware). Conflicts between performance and synthesis requirements should be expected and resolved early in the design phase through compromise.

There are many performance requirements which constrain the design of an electro-optical imaging system; however, four practical performance specifications tend to evolve from application requirements and drive most designs: sensitivity, resolution, spectral coverage, and area coverage rate.

Sensitivity: Defines the smallest *Signal* detectable in the presence of system noise.

Resolution: Defines the smallest resolvable object in the target plane at a given range-to-target, atmospheric condition and target signal level.

Spectral Coverage: The number of spectral bands and their associated spectral resolution needed to faithfully extract target information.

Area Coverage Rate: Amount of image area per unit time collected by the system at the given resolution.

Synthesis is the process (or art) of translating performance requirements into realizable and affordable hardware. Many synthesis requirements tend to be system and technology dependent, however several categories that apply to all systems include:

Cost: Is the approach within the customer's budget ?

Technical Feasibility: Is the approach technically feasible with appropriate levels of technology ?

Risk: The level of risk (technical feasibility assumed) that can be expected for a given design approach. Examples include system components that require unavailable or immature technology, and designs that rely on complex relationships with multiple contractors.

Schedule: Can system be completed in the customer allocated time.

Power, Size and Weight: Related to cost – especially in space and many airborne applications where weight, payload volume, and power constraints normally dominate a system.

Quality Control, Testability and Reliability: The quicker these categories are integrated into the early design cycle the better. Expect these items to consume a sizable fraction of the cost and schedule allocations.

While specifying performance and synthesis requirements may at first appear to be a waste of time, failure to clearly link customer-directed performance requirements to system synthesis requirements can lead to a wonderful design of the wrong system, wasting a good deal more time, not to mention money. **Section 2**, will discuss the analysis tools required for rapid system design, while **Section 3** presents a multi-spectral orbital imager design example that exercises the design methodology and applies many of the concepts discussed. For additional, comprehensive information concerning electro-optical systems design, the reader is urged to consult the available literature including *The Infrared and Electro-Optical Systems Handbook*[2], *Electro-Optical Imaging System Performance*[3], and *Electro-Optical Systems Performance Modeling*[4].

2. ELECTRO-OPTICAL IMAGING ANALYSIS

The analysis, schematically diagrammed in **Figure 2**, divides the problem into two parts: i) signal detection and ii) imaging quality and resolution. Signal detection evaluates detection efficiency in the presence of noise while imaging quality and resolution quantifies the efficiency in transmission of spatial information from target through electronic image capture. The two components can be combined to generate performance parameters for a given scene. (Note – the tools described in this section are intended for preliminary system level development and design, and include noise and OTF budgeting models for developing system tolerances. Though some of the models can be modified to do so, they were not developed for detailed, technology specific subsystem or component analysis.)

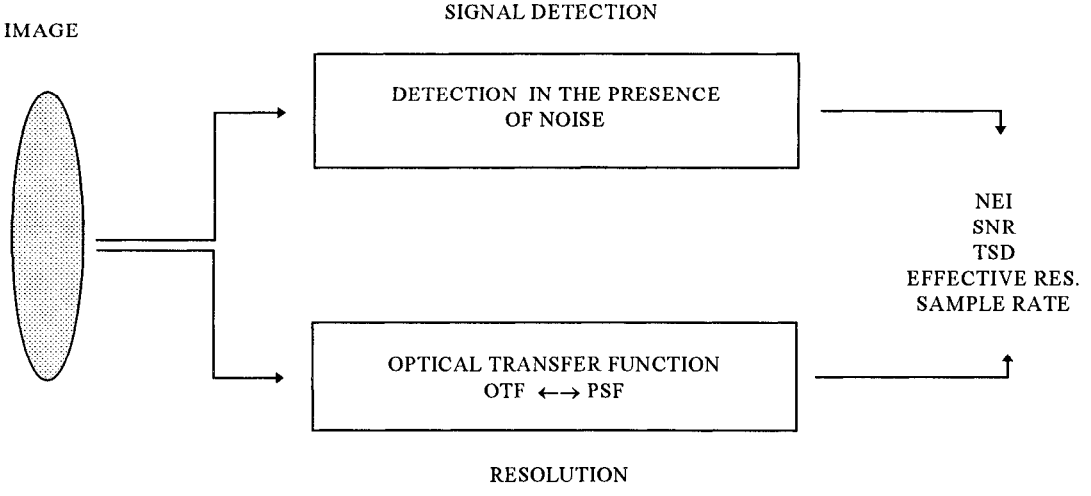

Figure 2. Electro-Optic Imaging Analysis Approach.

2.1. Signal detection in the presence of noise

2.1.1. Spectral transmission function

For the rapid development of multi-spectral systems, a spectral transmission function that will efficiently and realistically model the following parameters for each band is desired.

i) Average passband transmission.
ii) Average stopband transmission.
iii) Adjustable filter strength i.e. passband to stopband slope.
iv) Well defined band center and passband/stopband edges that do not shift as a function of filter strength.

Inherent in i) and ii) is the assumption that a band's spectral transmittance is sufficiently well behaved so that its passband and stopband can be represented by an equivalent average value. The transmission function that meets the above criteria and that will be used throughout the paper is defined as

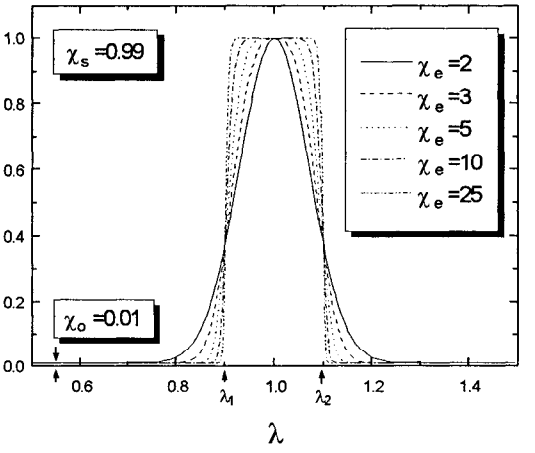

Figure 3. Spectral Transmission Function.

$$\chi(\lambda) = \chi_o + \chi_s \, e^{-\left|\frac{\lambda-\lambda_o}{\frac{\lambda_2-\lambda_1}{2}}\right|^{\chi_e}} . \qquad (2)$$

Where, referring to parameters i) - iv) above and **Figure 3**:

i) The average passband transmission, $\chi_s = T_o T_f$, is the product of optical train and filter transmissions.
ii) The average stopband transmission, χ_o, is typically on the order of 10^{-4} because many filter manufactures cannot readily measure below this value.
iii) Adjustable filter strength, χ_e, is the function's exponential coefficient that can range from a simple Gaussian filter for $\chi_e=2$, to an ideal filter for $\chi_e >> 10$. A good default value when starting an analysis is $\chi_e=4$.
iv) Well defined band center, $\lambda_o = \lambda_1 + \frac{\lambda_2 - \lambda_1}{2}$, and passband/stopband edges, λ_1 and λ_2 (1/e band-edges), that do not shift as a function of filter strength.

2.1.2. Signal irradiance at detector and detection spectral efficiency

Now that the transmission function is in place, the signal irradiance (given the signal spectral radiance), referenced at the detector, is evaluated by[5]

$$\Phi_s = \frac{\Omega_o}{h\,c}\int_{\lambda_1}^{\lambda_2} L_s(\lambda)\,\chi(\lambda)\,\lambda\,d\lambda \quad [\text{ph/m}^2\text{-s}], \qquad (3)$$

where

$\Omega_o = \left(1-\left(\frac{D_{obs}}{D_o}\right)^2\right)\cdot\frac{\pi}{4\cdot\left(\frac{f_l}{D_o}\right)^2}$ [sr], is the effective solid angle subtended by the optical aperture, D_o the diameter of clear aperture, D_{obs} the diameter of the clear aperture obstruction, f_l the effective system focal length , $L_s(\lambda)\,d\lambda$ [w/m^2-sr] the

signal spectral radiance, $h = 6.626\ 10^{-34}$ [J-s] is Plank's constant, and $c = 2.998\ 10^{8}$ [m/s] the speed of light. Note that instead of integrating over the limits $0 \rightarrow \infty$, the integration limit is over the transmission function band edges $\lambda_1 \rightarrow \lambda_2$, the reason becomes apparent when the detection spectral efficiency is considered. Detection spectral efficiency provides a measure of passband *Signal* to stopband *noise* and can be defined as

$$SE = \frac{\int_{\lambda_1}^{\lambda_2} \left[L_s(\lambda) + L_{bg}(\lambda)\right] \chi(\lambda)\, \eta_d(\lambda)\, \lambda\, d\lambda}{\int_{0}^{\infty} \left[L_s(\lambda) + L_{bg}(\lambda)\right] \chi(\lambda)\, \eta_d(\lambda)\, \lambda\, d\lambda} \cdot 100 \tag{4}$$

where $L_{bg}(\lambda)$ is the background spectral radiance and $\eta_d(\lambda)$ the detector quantum efficiency. Notice that the passband/stopband wavelengths, $\lambda_1 \rightarrow \lambda_2$, that differentiate between *Signal* and noise are rather arbitrary. For mathematical convenience, this paper defines the *Signal* bandwidth, $\lambda_1 \rightarrow \lambda_2$, as the 1/e transmission function band-edges. As long as it is consistently applied through an analysis, any other signal bandwidth can be defined i.e. $\lambda_1 \rightarrow \lambda_2$, at 50% transmission, 10% transmission or $1/e^2$ transmission etc. With *Signal* bandwidth defined, the effect of systematic noise, that may be introduced through out-of-band spectral leakage for a given signal and background radiance, can now be quantified. Spectral efficiencies of ~ 90% for most non-radiometric imaging applications are acceptable, while radiometric systems may typically require > 95% efficiencies. The spectral efficiency is manipulated by adjusting the transmission function parameters, λ_1, λ_2, χ_e and χ_o. Care should be taken to monitor the *Signal* SNR when adjusting the transmission function. When the "perfect" spectral efficiency of 99.9% is achieved, it may be at the expense of very low SNR. Practically, the detector has a finite response and the quantum efficiency, $\eta_d(\lambda)$, can be replaced by its average value, η_d, and the limits of the integral can be substituted for the effective quantum efficiency bandwidth, $\lambda_{\eta 1} \rightarrow \lambda_{\eta 2}$. The spectral efficiency reduces to

$$SE = \frac{\int_{\lambda_1}^{\lambda_2} \left[L_s(\lambda) + L_{bg}(\lambda)\right] \chi(\lambda)\, \lambda\, d\lambda}{\int_{\lambda_{\eta 1}}^{\lambda_{\eta 2}} \left[L_s(\lambda) + L_{bg}(\lambda)\right] \chi(\lambda)\, \lambda\, d\lambda} \cdot 100\,, \tag{5}$$

which simplifies prototyping and computer analysis (by removing the $0 \rightarrow \infty$ limit).

2.1.3. Noise analysis

System noise, as illustrated in **Figure 4**, can be broken into three primary components -- (1) photon noise, (2) detector, amplifier, readout, and processing noise, and (3) systematic noise. The signal-to-noise ratio *referenced at the detector*[6] is

$$SNR = \frac{\Phi_s}{NEI_{tot}}, \tag{6}$$

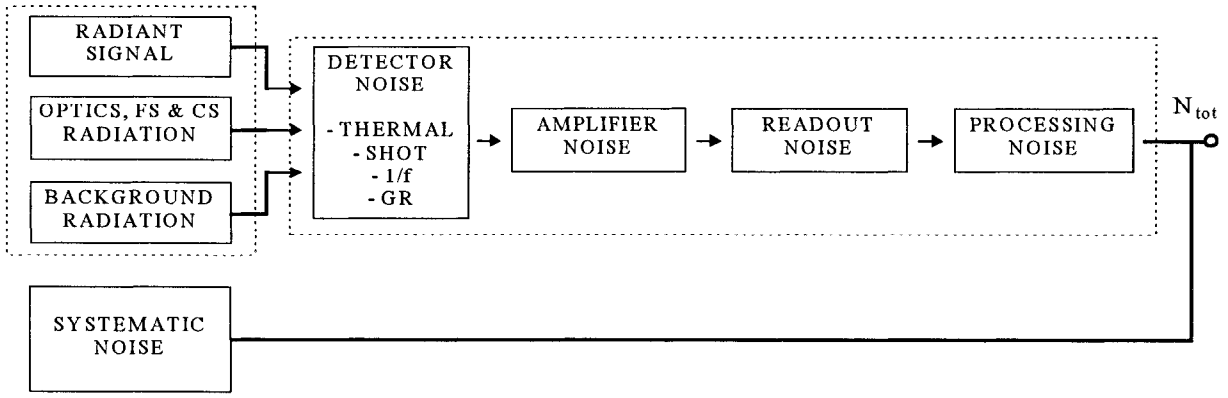

Figure 4. System Noise. Note: FS ≡ field-stop, CS ≡ cold-shield and GR ≡ generation recombination.

where:

Φ_s	signal irradiance,
$NEI_{tot} = \sqrt{NEI_{ph}^2 + NEI_{dar}^2 + NEI_{sys}^2}$	total noise equivalent irradiance,
$NEI_{ph}^2 = NEI_s^2 + NEI_{op}^2 + NEI_{fs}^2 + NEI_{cs}^2 + NEI_{bg}^2$	photon noise: signal + optics + field-stop + cold-shield + background,
$NEI_{dar}^2 = NEI_{\det}^2 + NEI_{amp}^2 + NEI_{ro}^2 + NEI_{dig}^2$	electronic noise: detector + amplifier + readout + digitization,
$NEI_{sys}^2 = NEI_{xt}^2 + ...$	systematic: cross-talk + ... etc.

All of the above noise equivalent irradiances are *referenced at the detector*. The selection of the surface of the detector as the SNR reference point needs some elaboration. When evaluating the system SNR, the *Signal* and system noise (σ_{system}) can be referenced at any point in the system – at the aperture, between the optical train and filter, at the detector, at the amplifier etc. This paper references the surface of the detector because it is an electro-optical system's natural *optical* $\leftrightarrow$ *electronic* interface. Everything to the "left" of the interface lies in the optical domain, while to the "right" in the electronic domain (the interface is illustrated in **Figure 4**, which falls between the dashed boxes).

The photon noise sources are diagrammed in **Figure 5**., where the optics, field-stop, and cold-shield are modeled as thermal sources, while signal and background radiances tend to cover the entire spectrum. Note that a good design requires proper matching of system and cold-shield solid angle. Hence, requires $\Omega_{cs} \sim \Omega_{sys}$, with

$$\Omega_{sys} = \frac{\pi}{4\left(\frac{f_l}{D_o}\right)^2} \text{ [sr]}.$$

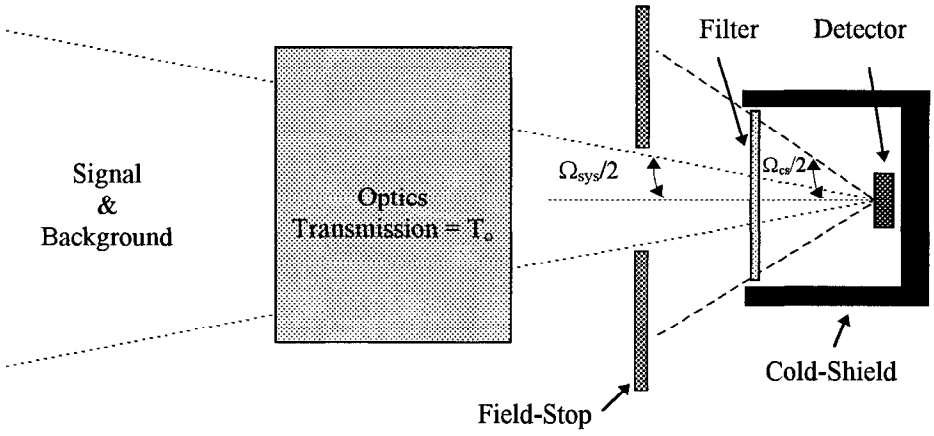

Figure 5. Photon Noise Sources.

Expressions evaluating the noise equivalent irradiance for signal, background, optical train, field-stop, and cold shield follow.

Signal:

$$NEI_s = \sqrt{\frac{\kappa_d \, \Delta f}{A_d \, \eta_d} \Phi_s} = \sqrt{\frac{\kappa_d \, \Delta f \, \Omega_o}{A_d \, \eta_d \, h \, c} \int_{\lambda_{\eta 1}}^{\lambda_{\eta 2}} L_s(\lambda) \, \chi(\lambda) \, \lambda \, d\lambda} \qquad \text{[ph/m}^2\text{-s]} \qquad (7)$$

Where Δf is the noise equivalent bandwidth in Hertz of the band, and is normally given by $\Delta f = (2\tau_o)^{-1}$, τ_o = effective integration time (single sample or multiple time delay and integrate samples may be used), A_d the detector area, and κ_d the noise process scale factor ($\kappa_d = 2$ for a photovoltaic and $\kappa_d = 4$ for photoconductor).

Background:

$$NEI_{bg} = \sqrt{\frac{\kappa_d \ \Delta f \ \Omega_o}{A_d \ \eta_d \ h \ c} \int_{\lambda_{\eta 1}}^{\lambda_{\eta 2}} L_{bg}(\lambda) \ \chi(\lambda) \ \lambda \ d\lambda} \qquad [\text{ph/m}^2\text{-s}] \qquad (8)$$

Optical Train:

$$NEI_{op} = \sqrt{\frac{\kappa_d \ \Delta f}{A_d \ \eta_d \ h \ c} \frac{\Omega_{sys}}{\pi} \int_{\lambda_{\eta 1}}^{\lambda_{\eta 2}} \sum_i M_{op}\left(T_{op_i}, \varepsilon_{op_i}, \lambda\right) \frac{\chi(\lambda)}{T_{o_i}} \lambda \ d\lambda} \qquad [\text{ph/m}^2\text{-s}] \qquad (9)$$

Where each optical element or optical subsystem, i=1,2,3,..n, contributes to the near-field thermal exitance M_{op}. Note how the remaining optical transmission from the i[th] component to the detector surface is maintained by dividing the system transmission $\chi(\lambda)$ by the i[th] component of T_o. In many cases, especially when designing a new system, *apriori* knowledge of the number, position, temperature, and material properties of the optical elements is unavailable. However, an NEI_{op} budget can be allocated by approximating the thermal exitance with a single source,

$$NEI_{op} = \sqrt{\frac{\kappa_d \ \Delta f}{A_d \ \eta_d \ h \ c} \frac{\Omega_{sys}}{\pi} \int_{\lambda_{\eta 1}}^{\lambda_{\eta 2}} M_{op}\left(T_{op}, \varepsilon_{op}, \lambda\right) \frac{\chi(\lambda)}{T_o} \lambda \ d\lambda} \qquad [\text{ph/m}^2\text{-s}]. \qquad (10)$$

Typically, an $\varepsilon_{op} \sim 0.05 - 0.1$ @ $T_{op} = 300$ K will suffice for uncooled optics, where ε_{op} = effective emissivity, and T_{op} [°K] is the effective temperature.

Field Stop:

$$NEI_{fs} = \begin{cases} 0 \quad if \quad \Omega_{cs} \le \Omega_{sys}, \quad else \\ \sqrt{\frac{\kappa_d \ \Delta f}{A_d \ \eta_d \ h \ c} \frac{\left(\Omega_{cs} - \Omega_{sys}\right)}{\pi} \int_{\lambda_{\eta 1}}^{\lambda_{\eta 2}} M_{fs}\left(T_{fs}, \varepsilon_{fs}, \lambda\right) \frac{\chi(\lambda)}{T_o} \lambda \ d\lambda} \end{cases} \qquad [\text{ph/m}^2\text{-s}] \qquad (11)$$

Cold-Shield:

$$NEI_{cs} = \sqrt{\frac{\kappa_d \ \Delta f}{A_d \ \eta_d \ h \ c} \frac{\left(\pi - \Omega_{cs}\right)}{\pi} \int_{\lambda_{\eta 1}}^{\lambda_{\eta 2}} M_{cs}\left(T_{cs}, \varepsilon_{cs}, \lambda\right) \frac{\chi(\lambda)}{T_o} \lambda \ d\lambda} \qquad [\text{ph/m}^2\text{-s}] \qquad (12)$$

The exitance functions, M_{op}, M_{fs}, and M_{cs} are of the form

$$M\left(T, \varepsilon, \lambda\right) d\lambda = \frac{2 \pi h c^2}{\lambda^5} \varepsilon \, e^{\frac{h c}{\lambda k_b T}} \, d\lambda \quad [\text{W/m}^2], \qquad (13)$$

where $k_b = 1.381 \ 10^{-23}$ [J/K] Boltzmann constant, ε = emissivity, and T [°K] = temperature. Signal and background radiances, $L_s(\lambda) \ d\lambda$ and $L_{bg}(\lambda) \ d\lambda$ [w/m^2-sr], from a given scene that include complex transmission, backscatter, and emission effects can be generated with computer simulation tools such as LOWTRAN or MODTRAN[7]. An optional analytical approach and discussion is given in the Appendix.

The remaining two noise terms, electronic NEI_{dar} and systematic NEI_{sys}, will not be pursued any further except within the context of establishing a synthesis-requirement noise budget based on top-level *Sensitivity* performance requirements (SNR analysis). As discussed in **Section 1.2.**, once an NEI_{dar} budget is defined, a technology-dependent feasibility study is performed to identify a candidate technology that meets the NEI_{dar} budget. If no appropriate candidate is found to fulfill the synthesis requirements, the system design is iterated until an acceptable compromise between performance and synthesis is achieved. The procedure of extracting a noise budget from scene-dependent SNR analysis will be explained in **Section 3**

through a detailed example. As a final observation, note that band leakage (detection spectral efficiency **Section 2.1.2**) is a form of *systematic* noise through spectral cross-talk.

Note that correlated noise (1/f, drift etc.) and white noise are not separated in the NEI terms. When large enough, this type of correlated noise must be reduced by system calibration in order to avoid imaging artifacts[8] and/or radiometric errors.

2.2. Optical resolution

Referring to **Figure 6**, the image chain shown is a schematic description of the primary optical elements from target image to output. The image forming process depicted in **Figure 6** must account for loss of image fidelity as a function of spatial frequency or spatial resolution. This degradation in fidelity is due to the aggregate degradation of the individual components shown in the boxes of **Figure 6**, and can be quantified by either a system optical transfer function (OTF) or by a point spread function (PSF), both of which are described in two dimensions. The final image captured by the imaging process is obtained by taking the convolution of the system PSF with the original object space image or multiplying the system OTF by the Fourier transform (FT) of the original input image and then inverse Fourier transforming (IFT) this product to obtain a final image. Note that there is the implicit assumption that the system is linear and that the system OTF and PSF form a Fourier transform pair. For a given input scene defined at band center wavelength, λ_o (see **Equation 2**), the output scene is[9, 10]:

Spatial Domain: $$\Phi_{image}(x,y,\lambda_o) = PSF_{sys}(x,y,\lambda_o) * \Phi_{target}(x,y,\lambda_o) \quad \textbf{(14)}$$

Frequency Domain: $$\Phi_{image}(x,y,\lambda_o) = IFT\{OTF_{sys}(k_x,k_y,\lambda_o)\cdot FT[\Phi_{target}(x,y,\lambda_o)]\} \quad \textbf{(15)}$$

where k_x and k_y [cycles/m] are the spatial frequency domain coordinates and the system OTF is evaluated as the product of the components in **Figure 6**,

$$OTF_{sys}(k_x,k_y,\lambda_o) = OTF_{sp}(k_x,k_y,\lambda_o)\cdot OTF_{a/r}(k_x,k_y,\lambda_o)\cdot OTF_{dd}(k_x,k_y,\lambda_o)\cdot OTF_{sa}(k_x,k_y,\lambda_o)\cdot OTF_{ta}(k_x,k_y,\lambda_o)\cdot OTF_{rv}(k_x,k_y,\lambda_o)\cdot \ldots$$
$$\ldots OTF_{df}(k_x,k_y,\lambda_o)\cdot OTF_{ab}(k_x,k_y,\lambda_o)\cdot OTF_{ap}(k_x,k_y,\lambda_o)\cdot OTF_{atm}(k_x,k_y,\lambda_o). \quad \textbf{(16)}$$

Note that evaluating the OTF at the band center frequency, λ_o, is only an approximation. For a spectrally broad band, a polychromatic[11] evaluation of the OTF may be required.

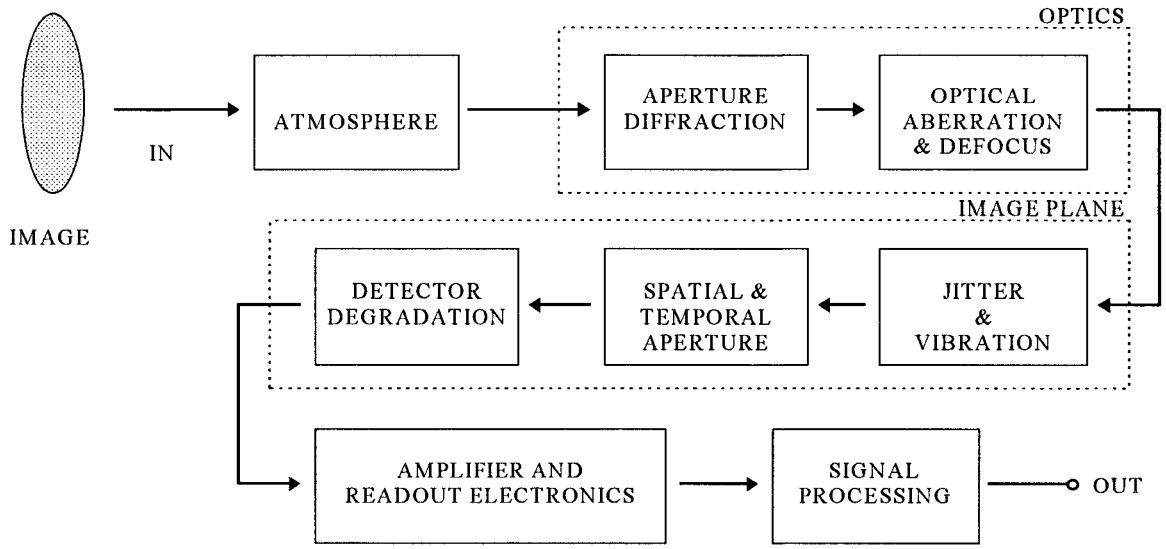

Figure 6. Imaging System.

In practice, the degradation components described in **Figure 6** are expressed analytically as component OTF's. Closed form mathematical models of these OTF's are available whereas the corresponding component PSF models tend to be mathematically intractable and are generally not available. **Section 2.2.1** lists a set of OTF's useful for analyzing the system components of **Figure 6**.

2.2.1. Optical transfer functions

Atmospheric: The optical transfer function for atmospheric turbulence is approximated by [12, 13, 14]

$$OTF_{atm}(k_r,\lambda) = e^{-3.44\left(\frac{1}{2\pi}\frac{\lambda f_l k_r}{\frac{\rho_o}{2.1}}\right)^{\frac{5}{3}}}, \tag{17}$$

with the atmospheric optical transverse coherence length (in meters) given by

$$\rho_o(\lambda) = \begin{cases} \left[1.46\left(\frac{2\pi}{\lambda}\right)\int_0^R C_n^2\left(h_o + |r\sin(\theta_s)|\right)\left(\frac{r}{R}\right)^{\frac{5}{3}} dr\right]^{-\frac{3}{5}} & \theta_s \le 0 \\ \left[1.46\left(\frac{2\cdot\pi}{\lambda}\right)\int_0^R C_n^2\left(h_o + |r\sin(\theta_s)|\right)\left(1-\frac{r}{R}\right)^{\frac{5}{3}} dr\right]^{-\frac{3}{5}} & otherwise, \end{cases} \tag{18}$$

where,

θ_s = slant angle (θ_s looking *up* through atmosphere, $-\theta_s$ looking *down* through atmosphere),
h_o = initial aperture or target height (lower of the two) [m],
R = aperture to target range [m],
C_n^2 = atmospheric refractive index structure factor [$m^{-2/3}$],
$k_r = \sqrt{k_x^2 + k_y^2}$ = spatial frequency [cycles/m].

Annular Aperture (O'Neill model):[15] For annular aperture of diameter D_o, a radial obstruction of diameter D_{obs}, and focal length f_l,

$$OTF_{ap}(k_r,\lambda) = \frac{I_1(k_r,\lambda) + I_2(k_r,\lambda) + I_3(k_r,\lambda)}{1 - \left(\frac{D_{obs}}{D_o}\right)^2} \tag{19}$$

where:

$$I_1(k_r,\lambda) = \begin{cases} \frac{2}{\pi}\left[\cos^{-1}\left(\frac{\lambda f_l k_r}{D_o}\right) - \frac{\lambda f_l k_r}{D_o}\sqrt{1-\left(\frac{\lambda f_l k_r}{D_o}\right)^2}\right], & 0 \le k_r \le \frac{D_o}{\lambda f_l} \\ 0, & k_r > \frac{D_o}{\lambda f_l} \end{cases} \tag{20}$$

$$I_2(k_r,\lambda) = \begin{cases} \frac{2}{\pi}\left(\frac{D_{obs}}{D_o}\right)^2\left[\cos^{-1}\left(\frac{\lambda f_l k_r}{D_{obs}}\right) - \frac{\lambda f_l k_r}{D_{obs}}\sqrt{1-\left(\frac{\lambda f_l k_r}{D_{obs}}\right)^2}\right], & 0 \le k_r \le \frac{D_{obs}}{\lambda f_l} \\ 0, & k_r > \frac{D_{obs}}{\lambda f_l} \end{cases}$$

$$I_3(k_r,\lambda)=\begin{cases} -2\left(\frac{D_{obs}}{D_o}\right)^2, & 0\le k_r\le\frac{D_o}{\lambda f_l}\left(1-\frac{D_{obs}}{D_o}\right) \\ -2\left(\frac{D_{obs}}{D_o}\right)^2+\frac{2D_{obs}}{\pi D_o}\sin(\Theta)+\frac{1+\left(\frac{D_{obs}}{D_o}\right)^2}{\pi}\Theta.... & \\ \quad -2\frac{1-\left(\frac{D_{obs}}{D_o}\right)^2}{\pi}\tan^{-1}\left[\left(\frac{1+\frac{D_{obs}}{D_o}}{1-\frac{D_{obs}}{D_o}}\right)\tan\left(\frac{\Theta}{2}\right)\right], & \frac{D_o}{\lambda f_l}\left(1-\frac{D_{obs}}{D_o}\right)<k_r\le\frac{D_o}{\lambda f_l}\left(1+\frac{D_{obs}}{D_o}\right) \\ 0, \quad k_r>\frac{D_o}{\lambda f_l}\left(1+\frac{D_{obs}}{D_o}\right) & \end{cases}$$

$$\Theta=\cos^{-1}\left[\frac{1+\left(\frac{D_{obs}}{D_o}\right)^2-\left(\frac{\lambda f_l k_r}{D_o}\right)^2}{2\frac{D_{obs}}{D_o}}\right].$$

Optical Aberrations: A detailed aberration analysis[16] or deviations from ideal paraxial behavior of an optical system requires a designed optical system to analyze. In view of this paper's focus on specifying the synthesis requirements of the optical system rather than optical design, an OTF function that will establish a total aberration budget is called for. A Gaussian distribution function, where the OTF is attenuated by e^{-1} at $k_r = \sigma_{ab}$ [cycles/m], is convenient and does reasonably well at approximating simple aberrations:[17]

$$OTF_{ab}(k_r,\lambda)=e^{-\left[\frac{k_r}{|\Delta_{ab}|\frac{D_o}{\lambda f_l}}\right]^2}, \tag{21}$$

where,

$\sigma_{ab} = \Delta_{ab}\dfrac{D_o}{\lambda f_l}$ [cycles/m],

Δ_{ab} = scale factor.

Note that at $\Delta_{ab} = 1$, the aberrations OTF is reduced by 1/e at the annular aperture cutoff $k_o = D_o/\lambda_o f_l$ [cycles/m], a convenient reference point when establishing a budget (OTF degradation is minimal at $\Delta_{ab} = 1$, while at $\Delta_{ab} = ½$ OTF degradation is quite noticeable).

Optical Defocus:[18] The defocus OTF approximates the effects of optical defocus depth and is useful in establishing focal depth tolerances:

$$OTF_{df}(k_r,\lambda)=\text{besinc}\left(\frac{1}{f_n^2}\Delta_{fs}\lambda\frac{k_r f_l}{D_o}\cdot\left(1-\frac{k_r\lambda f_l}{D_o}\right)\right), \tag{22}$$

with the focal depth given as $\Delta_{fs} x \lambda$ (the normalized focal shift is $\Delta_{fs} x f_n^{-2}$), and besinc(x) = 2 $J_1(\pi x)/\pi x$.

Random Vibration:[19] For an rms amplitude vibrational displacement of σ_v [m] (referenced to the image plane),

$$OTF_{rv}(k_r) = e^{-2\pi^2 \sigma_v^2 k_r^2}. \tag{23}$$

Use this OTF to establish system rms vibration and pointing stability tolerances. Note that this OTF does *not* properly account for systematic motion and various harmonic resonances which tends to vary from system to system. The rms pointing stability is given by $tan^{-1}(\sigma_v / f_l)$ [radians].

Spatial Aperture:[20] The two-dimensional trapezoidal spatial quantization of square pixels in the image plane is

$$OTF_{sa}(k_x, k_y) = \text{sinc}(k_x\ \Delta x)\ \text{sinc}(k_x\ (\Delta x - \delta x))\ \text{sinc}(k_y\ \Delta y)\ \text{sinc}(k_y\ (\Delta y - \delta y)), \tag{24}$$

where:

sinc(x)=sin(πx)/πx,
$\Delta x, \Delta y$ = pixel pitch [m],
$\delta x = \Delta x\ FF_x, \delta y = \Delta y\ FF_y$ = pixel dimension [m],
FF_x, FF_y = fill factor.

Temporal Aperture:[21] Degradation due to relative motion between the target and image plane, and TDI synchronism error between target motion and TDI image plane electronic scan rate and discrete charge motion effects (CCD only) is determined through

$$OTF_{ta}(k_x, k_y) = \text{sinc}\left[\frac{\tau_o\ f_l}{n_{cp}\ R}\left(k_x(V_x + \Delta V_x) + k_y(V_y + \Delta V_y)\right)\right] \frac{\text{sinc}\left[\frac{\tau_o\ f_l}{R}\left(k_x\ \Delta V_x + k_y\ \Delta V_y\right) n_{tdi}\right]}{\text{sinc}\left[\frac{\tau_o\ f_l}{R}\left(k_x\ \Delta V_x + k_y\ \Delta V_y\right) \frac{1}{n_{cp}}\right]}, \tag{25}$$

where:

sinc(x)=sin(πx)/πx,
R = aperture to target range [m],
f_l = effective focal length [m],
V_x, V_y = relative differential velocity between image-plane and target [m/s],
τ_o = integration period [s].

The following apply only to scanning TDI focal planes:

n_{tdi} = number of TDI stages,
n_{cp} = number of clock phases per sample (CCD only),
ΔV_x, ΔV_y = relative velocity error [m/s] between target and TDI image plane electronic scan rate and discrete charge motion effects (CCD only), else default to $n_{tdi} = n_{cp} = 1$, and $\Delta V_x = \Delta V_y = 0$.

The remaining OTF components depicted in **Figure 6** including detector carrier diffusion in CCD focal plane arrays,[22, 23, 24] detector, amplifier and readout bandwidth limitations, and OTF deficiencies that can be can be partially compensated for with signal processing [25, 26] are technology specific, and with the possible exception of carrier diffusion, are not included at the preliminary synthesis requirements level. The effects of these OTF components *should* be considered as the system design progresses towards a specific hardware technology.

2.2.2. Target sampled distance, effective resolution, and sampling criteria

For rapid performance analysis and synthesis of multi-spectral imaging systems, the raw OTF/PSF information generated for each band from **Equations 14 -25** should be processed and reduced to a set of parameters that efficiently summarizes imaging system performance. While the ability to examine each and every OTF/PSF component for a given band is necessary (especially when analyzing resolution limits and during optimization sessions), the information overload generated by a large, multi-band system is definitely overwhelming and generally not conducive to efficient analysis. A reduced set of representative parameters will aid in flagging and identifying problems at the systems level without information overload. The parameters, target sampled distance, effective resolution, and sample rate are defined in the remainder of this section and applied to the example given in **Section 3**.

Target Sampled Distance (TSD): The TSD is geometric-optics projection of the pixel in the image plane onto the target. For pixel pitch Δx, Δy, range-to-target R, and effective system focal length f_l, the projected TSD in Cartesian coordinates is

$$TSD_x = \Delta x \frac{R}{f_l}, \qquad TSD_y = \Delta x \frac{R}{f_l}. \tag{26}$$

Related to the TSD is the number of pixels or samples required to cover the target area given by the product of $L_x L_y$

$$N_{pix\_x} = \frac{L_x}{TSD_x}, \qquad N_{pix\_y} = \frac{L_y}{TSD_y}. \tag{27}$$

Hence, for a fixed target area coverage rate, **Equation 27** indicates a trade between resolution and the number of pixels/samples required. Note that the number pixels/samples determines the system data collection processing rate and storage requirements, which can become important system limitations.

Effective Resolution: The TSD can also be thought of as the geometric-optics projection of the spatial-aperture PSF, PSF_{sa} (IFT of **Equation 24**), onto the target. Considering the composition of OTF_{sys} given in **Equation 16**, the TSD is generally not an accurate representation of the imaging systems effective resolution due to probable contributions from other OTF components. A preferred measure of resolution is one that incorporates the full system OTF/PSF. Shade's equivalent pass band [3] approach estimates the PSF spread by evaluating the OTF's equivalent bandwidth and inverting,

$$\Delta_{psf\_x} = \frac{1}{2\int_0^{\infty} \left|OTF_{sys}(k,0,\lambda_o)\right|^2 dk}, \qquad \Delta_{psf\_y} = \frac{1}{2\int_0^{\infty} \left|OTF_{sys}(0,k,\lambda_o)\right|^2 dk}. \tag{28}$$

This concept is very similar to the noise equivalent bandwidth approach used when relating pulsewidth and noise bandwidth (see also Fourier uncertainty principle that can be found in most communication text books). While this technique is appropriate for most well-behaved OTF's, a second technique that operates directly on the PSF should be considered as a cross-check. The integrated intensity effective resolution integrates over the intensity of the PSF

$$\Delta_{psf\_x} = 2\xi, \quad given \quad \frac{\int_0^{\xi} \left|PSF_{sys}(x,0)\right| dx}{\int_0^{\infty} \left|PSF_{sys}(x,0)\right| dx} = 1 - \Delta I, \quad \Delta_{psf\_y} = 2\xi, \quad given \quad \frac{\int_0^{\xi} \left|PSF_{sys}(0,y)\right| dy}{\int_0^{\infty} \left|PSF_{sys}(0,y)\right| dy} = 1 - \Delta I. \tag{29}$$

where ΔI is the fractional integrated intensity error (typically ~ 0.05). For well behaved OTF/PSF's both the Shade's equivalent pass band and the integrated intensity evaluate PSF spreads will differ by only a few percent.

Finally, the target-projected effective resolution, given a point source is

$$RES_x = \Delta_{psf\_x}\frac{R}{f_l}, \qquad RES_y = \Delta_{psf\_y}\frac{R}{f_l}. \tag{30}$$

Note that the effective resolution RES approaches the pixel TSD when PSF_{ta} dominates the system point spread function.

The diameter of the first zero of the Airy pattern of a circular aperture's PSF is a familiar measure and will be applied in the following sampling criteria and in **Section 3**. Applying the inverse Fourier transform to the Circular aperture portion of **Equation 20** (D_{obs} =0) and solving for the first zero,

$$\pi\left(\frac{D_o}{2}\right)^2 \text{besinc}\left(\frac{k\,D_o\,r}{2\,\pi\,f_l}\right)^2 \to 0 \quad @ \quad r \approx 1.22\frac{\lambda\,f_l}{D_o}, \quad k = \frac{2\,\pi}{\lambda},$$

results in an Airy disk diameter of $\delta_{ap} = 2.44\frac{\lambda\,f_l}{D_o}$. **(31)**

Sampling Criteria: For the unique reconstruction of a sampled image, the Whittaker-Shannon sampling theorem[9, 27, 28, 29] requires a uniform sample spacing of no less than

$$\Delta x = \frac{1}{2\,k_n}, \tag{32}$$

where k_n is the highest resolvable spatial frequency contained the image. The sample rate of $2k_n$ [cycles/m] is known as the Nyquist rate and

$$k_n = \frac{1}{2\,\Delta x} \tag{33}$$

the Nyquist frequency. Any spatial frequencies below the Nyquist frequency will be unambiguously reconstructed while spatial frequencies above the Nyquist frequency may be *aliased*[30, 31] to a lower frequency. Applying the sampling theorem to the circular aperture portion of **Equation 20** (D_{obs} = 0), the high-frequency cutoff, k_o, is $k_o = \frac{D_o}{\lambda\,f_l}$.

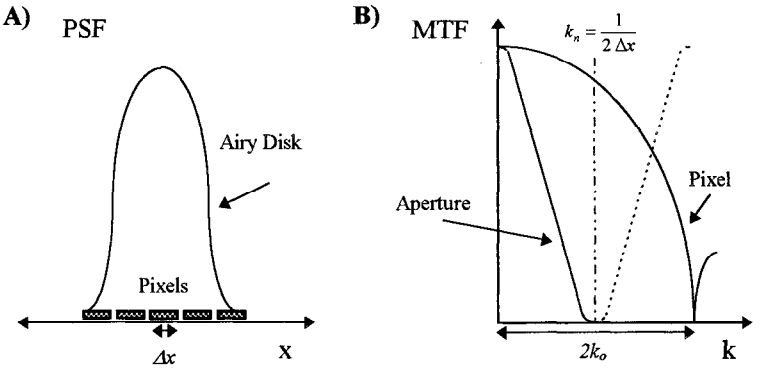

Figure 7. Spatial and Frequency Domain Illustration of a Nyquist Sampled Circular Aperture: A) 4.88 pixels per dimension under the Airy disk, and **B)** aperture cutoff, k_o, equal to the pixel Nyquist frequency, k_n, which is half the Nyquist rate of $2k_o$. Sampling at a rate of less then $2k_o$ can overlap and alias the adjacent spectra (dotted curve) about the Nyquist frequency k_n.

From **Equation 32**, Nyquist sampling requires

$$\Delta x = \Delta y = \frac{\lambda\,f_l}{2\,D_o}, \tag{34}$$

where Δx and Δy are the pixels dimensions defined in **Equation 24** (100% fill factor assumed). The number of pixels under the Airy disk diameter from **Equation 31** is then

$$\frac{\delta_{ap}}{\Delta x} = \frac{\delta_{ap}}{\Delta y} = \frac{2.44\frac{\lambda\,f_l}{D_o}}{\frac{\lambda\,f_l}{2\,D_o}} = 4.88 \quad \text{pixels.} \tag{35}$$

Figure 7 illustrates the spatial and frequency domain representation of a Nyquist sampled circular aperture.

The sampling theorem can next be applied to the general optical OTF

$$OTF_o(k_x,k_y,\lambda_o) = OTF_{rv}(k_x,k_y,\lambda_o)\cdot OTF_{df}(k_x,k_y,\lambda_o)\cdot OTF_{ab}(k_x,k_y,\lambda_o)\cdot OTF_{ap}(k_x,k_y,\lambda_o)\cdot OTF_{atm}(k_x,k_y,\lambda_o), \tag{36}$$

by developing an equivalent PSF spread sampling criteria. The equivalent PSF spread of the circular aperture (**Equation 20** $D_{obs} = 0$) using Shade's equivalent pass band evaluates to

$$\Delta_{cir} = \frac{1}{2\int_0^\infty \left|OTF_{ap\_cir}\right|^2 dk} = \left[2\int_0^\infty \left|\frac{2}{\pi}\left(\cos^{-1}(r) - r\sqrt{1-r^2}\right)\right|^2 dr\right]^{-1} \frac{\lambda f_l}{D_o} = 1.835\frac{\lambda f_l}{D_o}, \tag{37}$$

where 1.835 is the circular aperture form factor. The sampling theorem requires,

$$\frac{\Delta_{cir}}{\Delta x} = \frac{\Delta_{cir}}{\Delta y} = \frac{1.835\dfrac{\lambda f_l}{D_o}}{\dfrac{\lambda f_l}{2\,D_o}} = 3.67, \tag{38}$$

and, an equivalent sampling rate can be estimated with

$$S_{r\_x} = \frac{\Delta_o}{3.67\,\Delta x}, \qquad S_{r\_y} = \frac{\Delta_o}{3.67\,\Delta y}, \tag{39}$$

where from **Equation 36**

$$\Delta_o = \frac{1}{2\int_0^\infty \left|OTF_o(k,0,\lambda_o)\right|^2 dk}. \tag{40}$$

A sample rate (S_r) of 1.0 implies Nyquist rate sampling with 4.88 pixels per Airy disk diameter per dimension as illustrated in **Figure 7**. Approximately twenty pixels per Airy disk is a costly proposition and is probably unnecessary for most applications. A sample rate of 0.2 to 0.5 (one to three pixels per Airy disk diameter) should be used as a synthesis target for imaging systems with nominal resolution and aliasing requirements. Sample rates of 0.5 to 1.0 should be considered for high resolution systems or when imaging scenes contain high spatial uniformity.

A more complete definition of the sample rate would account for the image-plane spatial and temporal aperture OTF degradation. Hence,

$$S_{r\_x} = \frac{\Delta_o}{3.67\,\Delta_{ip\_x}}, \qquad S_{r\_y} = \frac{\Delta_o}{3.67\,\Delta_{ip\_y}}, \tag{41}$$

where

$$\Delta_{ip\_x} = \frac{1}{2\int_0^\infty \left|OTF_{ip}(k,0,\lambda_o)\right|^2 dk}, \qquad \Delta_{ip\_y} = \frac{1}{2\int_0^\infty \left|OTF_{ip}(0,k,\lambda_o)\right|^2 dk}, \tag{42}$$

and $OTF_{ip}(k_x,k_y,\lambda_o) = OTF_{sa}(k_x,k_y,\lambda_o)\cdot OTF_{ta}(k_x,k_y,\lambda_o)$. (43)

The implications of **Equation 41** have yet to be fully investigated, therefore the sample rate definition given by **Equation 39** will be used in **Section 3**.

3.0 EXAMPLE: EIGHT BAND ENVIROMENTAL IMAGER

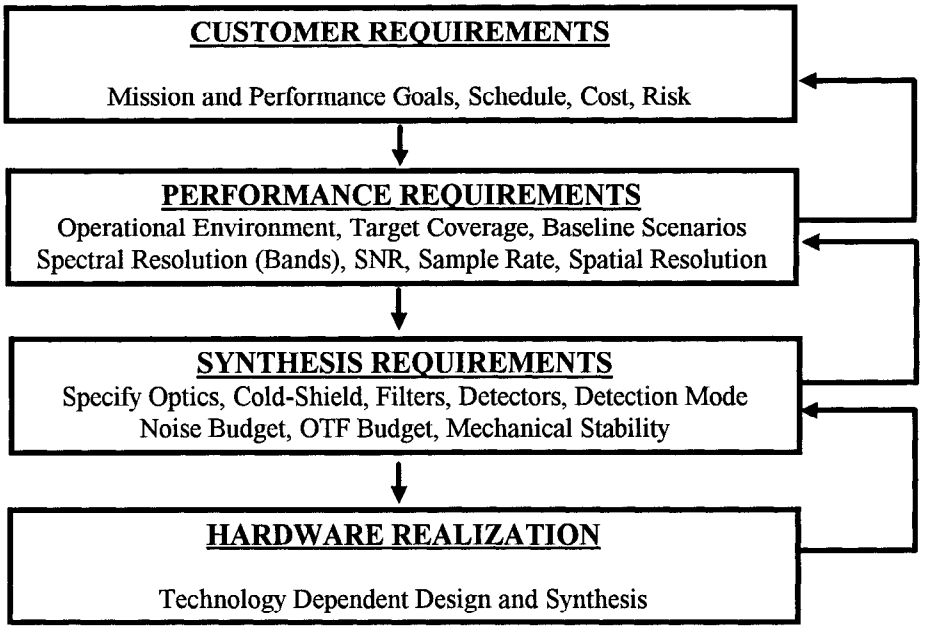

Figure 8. Summary of Methodology.

Figure 8 summarizes the methodology discussed in **Section 1**. Beginning with top-level customer-dictated system performance requirements and constraints, the critical system and component parameters (synthesis requirements) are derived, performance analyzed and iterated until a preliminary design, that meets customer requirements, is generated. In the following example, a fictional customer requests a preliminary study on the feasibility and system requirements (read synthesis requirements) of an environmental orbital imager. The example is rather simplistic with several assumption left unjustified (i.e. the remote sensing physics). However, within the context of the paper, this example should serve the purpose of illustrating the methodology.

3.1. Customer requirements

As an example, we will address the needs of a hypothetical customer who needs an environmental imaging system to:

- Monitor inland and coastal water quality, vegetation and surface temperature.
- Provide global coverage.
- Operate in daylight – require ~ 100:1 signal to noise ratio given lowest expected scene radiance (quantified later in **Figure 9**).
- Retrieve surface temperature with less than 5° K error at a 100 - 200 m feature resolution, and resolve water/vegetation features to less than 50 m. Assume irregular (natural) features for both temperature and water/vegetation. A target coverage of 20 km by 20 km is desired.

Before the synthesis requirements can be established, the customer requirements must be translated into a concise set of performance requirements.

3.2. Performance requirements

As a preliminary translation of customer requirements, the satellite will be placed in a polar orbit at an altitude of 500 km with an orbital velocity (Kepler's 3rd law) of $V_x = 7.06$ km/s, and a ground swath of 20 km. The imager will operate in a pushbroom mode with 'x' the along-scan axis and 'y' the cross-scan. For the purpose of reader familiarity, the spectral bands have been borrowed from LANDSAT and MODIS, and spatial resolutions are commensurate with a relatively modest telescope of about 0.3 m aperture.

Table 1. Targeted Performance Requirements

Band	λ_1 [μm]	λ_2 [μm]	SNR	Resolution [m]	Description
A	0.45	0.52	100	15	Blue - Water Quality
B	0.52	0.60	100	15	Green - Water Quality
C	0.63	0.69	100	15	Red - Water/Vegetation
D	0.76	0.86	100	15	Vegetation
E	2.08	2.35	100	30	Atmospheric Correction
F	3.929	3.989	100	60	Surface Temperature
G	10.78	11.28	100	60	Surface Temperature
H	11.77	12.27	100	60	Surface Temperature

The minimum SNR requirements (see **Equation 6**) must be met for the 'Lo' signal radiance conditions of **Figure 9**, and 'Resolution' refers to the effective point-source response given by **Equation 28** or **Equation 29**, with the criteria that of point source samples per scene feature.

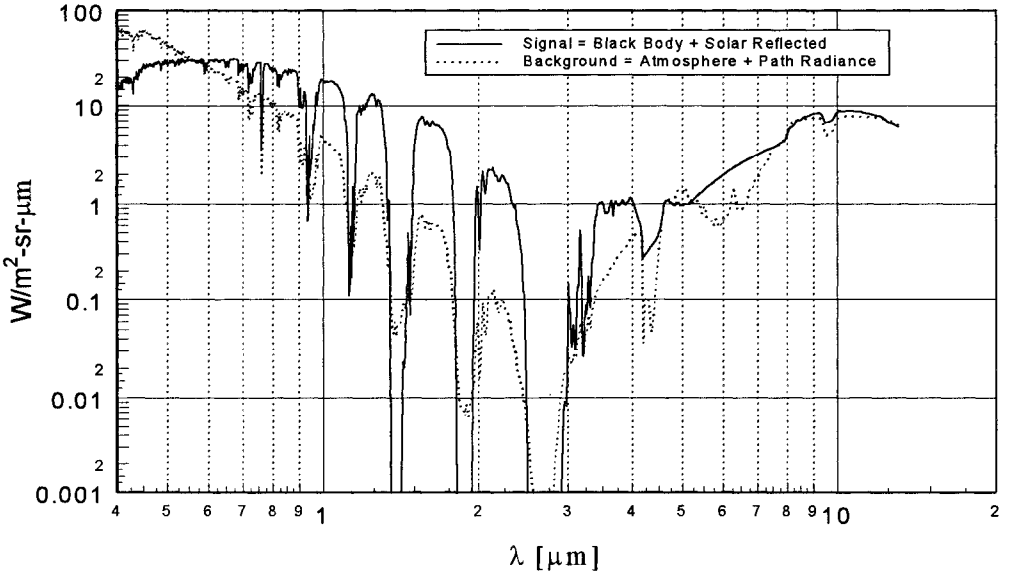

Figure 9. 'Lo' Signal and Background Radiance (Mid Latitude Summer, 23 km Visibility, 20 % Albedo, 30° Solar Elevation, Black Body: Temperature = 275 K @ emissivity = 0.8).

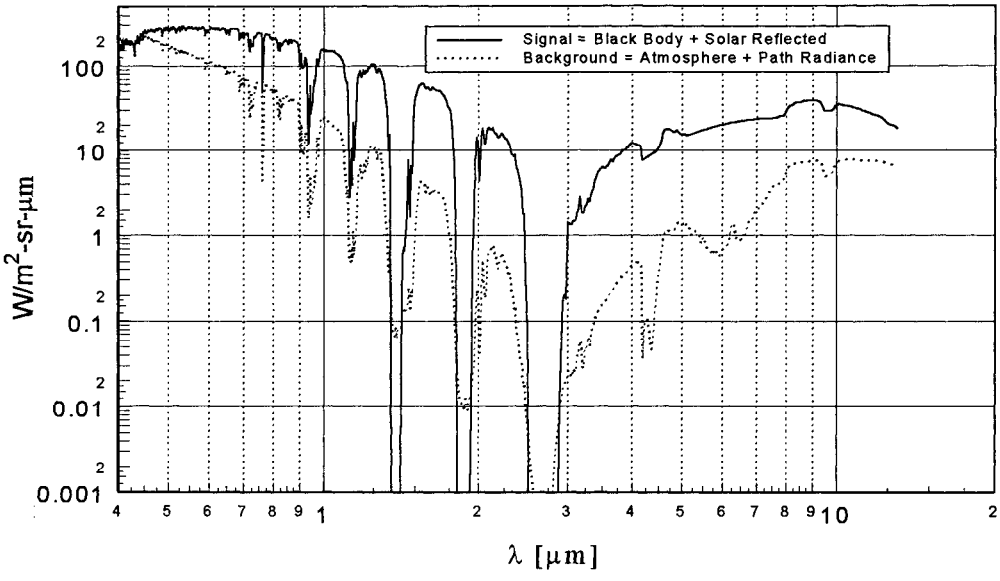

Figure 10. 'Hi' Signal and Background Radiance (Mid Latitude Summer, 23 km Visibility, 80 % Albedo, 75° Solar Elevation, Black Body: Temperature = 375 K @ emissivity = 0.8).

3.3. Iterate synthesis requirements

Establish Baseline

For the first iteration, the following steps are taken.

- Start the system iteration with Band H, because the longest wavelength will set the optical requirements. Select a Band H pixel pitch and a target sampled distance (TSD) that is a little less than the spatial resolution requirements. For this paper's example, TSD = 50 m, and $\Delta x = 50$ μm.

- Given that the longest wavelength in Band H is $\Lambda_o = 12.3$ μm, the minimum system aperture diameter and effective F# required to project the 50 m TSD onto the 50 μm pixel at an orbital height of 500 km is

$$D_o = 2.44\, R \frac{\Lambda_o}{TSD} = 30\ cm, \qquad F\# = \frac{\Delta_p}{2.44\, \Lambda_o} = 1.666 \cdot$$

- Check the optical sample rate (**Equation 35**)

$$S_r = \frac{F\#\, \Lambda_o}{2\, \Delta_p} = 0.21 \cdot$$

An $S_r = 0.21$ *Should* be acceptable given that the scene surface features are irregular (remember, the system is Nyquist sampled for $S_r \geq 1$).

- Finally, evaluate the preliminary system response to the "Lo" radiance given the diffraction limited optics of $D_o = 30$ cm and F# 1.67. Establish, through iteration, the SNR and resolution baseline.

Additional baseline assumptions include: off-axis optics ($D_{obs} = 0$), T_{FPA}, $T_{cold\ Shield} = 77$ K @ $\varepsilon = 1.0$, $T_{Optics} = 300$ K $\varepsilon = 0.05$, and a filter stopband leakage of 10^{-4}. The FPA assumptions are given in **Table 2.**

Table 2. FPA Assumption

Band	$\lambda_{\eta 1}$ [μm]	$\lambda_{\eta 2}$ [μm]	T_o	T_f	η_d	Pixel Pitch [μm]	Fill Factor
A	0.4	1	0.75	0.75	0.75	12.5	0.98
B	0.4	1	0.75	0.75	0.75	12.5	0.98
C	0.4	1	0.75	0.75	0.75	12.5	0.98
D	0.4	1	0.75	0.75	0.75	12.5	0.98
E	1	5	0.75	0.75	0.75	25	0.98
F	1	5	0.75	0.75	0.75	50	0.98
G	8	13	0.75	0.75	0.75	50	0.98
H	8	13	0.75	0.75	0.75	50	0.98

The pixel integration and noise equivalent bandwidth are calculated with

$$Pixel\ Integration\ time \equiv \tau_o = Pixel\ Pitch \cdot Fill\ Factor \frac{R}{f_l V_x}, \quad Noise\ BW \equiv \Delta f = \frac{1}{2\tau_o}.$$

Table 3. 1st Iteration Performance Summary

Band	SNR	%SE	S_r	TSD [m]	RES_x [m]	RES_y [m]	N_{pix}
A	210	93	0.06	12.5	20	13	1600
B	280	93	0.06	12.5	20	13	1600
C	300	93	0.07	12.5	20	13	1600
D	400	93	0.08	12.5	20	13	1600
E	1000	95	0.09	25	40	26	800
F	1200	92	0.09	50	80	51	400
G	14000	93	0.2	50	91	68	400
H	14000	93	0.2	50	93	71	400

The 1st iteration (**Table 3.**) produced a good SNR but a low effective resolution and sample rate (S_r). Note that the along-track resolution (RES**x**) suffers by pixel smear over the time τ_o (see **Equation 25**, the imager's relative target/pixel motion). Only through over-sampling by 2-4 samples per TSD can the along-track resolution approach the cross-track resolution. Since this will introduce a commensurate increase in data rate and processing requirements, a compromise between along-track and cross-track resolution is recommended. Hence, split the difference by straddling the resolution requirement. To increase resolution, trade-off a reduced SNR and increased N_{pix} for improved resolution by increasing the system F# from 1.67 to 2.0.

Table 4. 2nd Iteration Performance Summary

Band	SNR	NEI_{tot}	%SE	S_r	TSD [m]	RES_x [m]	RES_y [m]	N_{pix}
A	160	$2.8 \cdot 10^{15}$	93	0.06	10.4	16	11	1920
B	210	$2.9 \cdot 10^{15}$	93	0.07	10.4	17	11	1920
C	230	$2.4 \cdot 10^{15}$	93	0.08	10.4	17	11	1920
D	300	$2.8 \cdot 10^{15}$	93	0.09	10.4	17	11	1920
E	770	$6.5 \cdot 10^{14}$	95	0.1	20.8	34	22	960
F	930	$1.4 \cdot 10^{14}$	92	0.09	41.7	67	44	480
G	10000	$2.1 \cdot 10^{15}$	93	0.3	41.7	79	62	480
H	10000	$2.2 \cdot 10^{15}$	93	0.3	41.7	82	65	480

The 2nd iteration shows that, even though the sample rate (S_r) is a little on the low side, the system currently meets customer requirements. For the next, include an electronic noise budget for (NEI_{dar} **Equation 6**), and an OTF budget for aberrations (**Equation 21**), defocus (**Equation 22**), and pointing stability (rms vibrations **Equation 23**). In addition, increase filter strength of surface temperature bands F,G and H for a spectral efficiency of $\geq 95\%$. This will improve temperature resolution by reducing systematic noise due to band leakage. The results of this final iteration are summarized in **Table 5** and **Table 6**.

Table 5. Final Performance Summary for "Lo" Radiance

Band	SNR	%SE	$d\chi/d\lambda$	S_r	TSD [m]	RES_x [m]	RES_y [m]	N_{pix}
A	120	93	24	0.1	10.4	17	11	1920
B	160	93	21	0.1	10.4	17	11	1920
C	160	93	28	0.1	10.4	17	11	1920
D	230	93	17	0.1	10.4	17	12	1920
E	190	95	6	0.1	20.8	34	23	960
F	140	95	56	0.1	41.7	68	45	480
G	2300	96	5	0.3	41.7	80	62	480
H	2300	96	5	0.3	41.7	82	65	480

The filter slope, $d\chi/d\lambda$ is evaluated at the filter1/e points. Note that filter "F" may be difficult to realize.

Table 6. Noise and OTF Budget

Band	NEI_{dar} [ph/m^2-s]	NEC_{dar} [e]	σ_{ab}[cycles/mm]	Z_{focus} [μm]
A	$2.5 \cdot 10^{15}$	410	520	5
B	$2.5 \cdot 10^{15}$	410	450	6
C	$2.5 \cdot 10^{15}$	410	380	7
D	$2.5 \cdot 10^{15}$	410	310	8
E	$2.5 \cdot 10^{15}$	3300	170	11
F	$1 \cdot 10^{15}$	$1 \cdot 10^{4}$	95	20
G	$1 \cdot 10^{16}$	$1 \cdot 10^{5}$	45	28
H	$1 \cdot 10^{16}$	$1 \cdot 10^{5}$	42	30

σ_{ab} is the standard deviation of optical aberration budget (**Equation 21**), and Z_{focus} the ± focal depth tolerance (**Equation 22**). Finally, the pointing stability must be less than ±1 μrad to achieve resolution requirements.

Finally, the 'Hi' scene radiance of Figure 10 is run to set the dynamic range and to check the spectral efficiency of the filters. The results are tabulated in **Table 7** and **Table 8**.

Table 7. Performance Summary Given "Hi" Radiance

Band	SNR	%SE	S_r	TSD [m]	RES_x [m]	RES_y [m]	N_{pix}
A	580	93	0.1	10.4	17	11	1920
B	730	93	0.1	10.4	17	11	1920
C	700	93	0.1	10.4	17	11	1920
D	900	93	0.1	10.4	17	12	1920
E	1300	95	0.1	20.8	34	23	960
F	1300	95	0.1	41.7	68	45	480
G	8000	96	0.3	41.7	80	62	480
H	7300	96	0.3	41.7	82	65	480

Table 8. Dynamic Range Requirements Given "Lo" & "Hi" Radiance

Band	SNR_{lo}	$\Phi_{s\ lo}$ [ph/m^2-s]	$Q_{p\ lo}$ [e]	SNR_{hi}	$\Phi_{s\ hi}$ [ph/m^2-s]	$Q_{p\ hi}$ [e]
A	120	$4.4 \cdot 10^{17}$	$2.9 \cdot 10^{5}$	580	$4.2 \cdot 10^{18}$	$1.2 \cdot 10^{6}$
B	160	$6.2 \cdot 10^{17}$	$2.2 \cdot 10^{5}$	730	$5.8 \cdot 10^{18}$	$1.5 \cdot 10^{6}$
C	160	$5.5 \cdot 10^{17}$	$1.6 \cdot 10^{5}$	700	$4.9 \cdot 10^{18}$	$1.1 \cdot 10^{6}$
D	230	$8.5 \cdot 10^{17}$	$2.1 \cdot 10^{5}$	900	$7.4 \cdot 10^{18}$	$1.6 \cdot 10^{6}$
E	190	$5.0 \cdot 10^{17}$	$7.2 \cdot 10^{5}$	1300	$4.2 \cdot 10^{18}$	$5.9 \cdot 10^{6}$
F	140	$1.4 \cdot 10^{17}$	$2.0 \cdot 10^{6}$	1300	$1.4 \cdot 10^{18}$	$1.6 \cdot 10^{7}$
G	2300	$2.3 \cdot 10^{19}$	$5.0 \cdot 10^{8}$	8000	$8.4 \cdot 10^{19}$	$1.2 \cdot 10^{9}$
H	2300	$2.3 \cdot 10^{19}$	$5.2 \cdot 10^{8}$	7300	$7.7 \cdot 10^{19}$	$1.1 \cdot 10^{9}$

Φ_s is the signal irradiance (**Equation 3**) and Q_p the total integrated photon charge (signal + background + optics + field-stop + cold-shield).

A summary of the final synthesis requirements follows in **Table 9**. The next step, of course, involves technology dependent hardware realization, which are beyond the immediate capabilities of the tools discussed in this paper. However, the methodology remains the same: the technology dependent point design and analysis of components and subsystems must still meet top-level, customer-dictated performance and synthesis requirements.

Table 9. Summary of Synthesis Requirements

Off-Axis Optics: D_o = 30 cm and F# 2.0, T_{FPA}, $T_{Cold\ Shield}$ = 77 K ε = 1.0, T_{Optics} = 300 K ε = 0.05,
Pointing Stability $\leq \pm 1$ μrad

Band	λ_1 [μm]	λ_2 [μm]	τ_e	τ_o	T_o	T_f	$\Delta x,y$ [μm]	$FF_{x,y}$	η_d	λ_{n1} [μm]	λ_{n2} [μm]	τ_n [ms]
A	0.45	0.52	4	10^{-4}	0.75	0.75	12.5	0.98	0.75	0.4	1	1.446
B	0.52	0.60	4	10^{-4}	0.75	0.75	12.5	0.98	0.75	0.4	1	1.446
C	0.63	0.69	4	10^{-4}	0.75	0.75	12.5	0.98	0.75	0.4	1	1.446
D	0.76	0.86	4	10^{-4}	0.75	0.75	12.5	0.98	0.75	0.4	1	1.446
E	2.08	2.35	4	10^{-4}	0.75	0.75	25	0.98	0.75	1	5	2.891
F	3.929	3.989	8	10^{-4}	0.75	0.75	50	0.98	0.75	1	5	5.782
G	10.78	11.28	6	10^{-4}	0.75	0.75	50	0.98	0.75	8	13	5.782
H	11.77	12.27	6	10^{-4}	0.75	0.75	50	0.98	0.75	8	13	5.782

Noise & OTF budgets and focal depth tolerance summarized in **Table 6**, and dynamic range in **Table 8**.

4.0 CONCLUSION

The analysis methodology and corresponding analytical tools for rapid top-down design of multi-spectral imaging systems have been presented. Beginning with top-level customer-dictated system performance requirements and constraints, the approach discussed in this paper provided for the derivation, analysis and iteration of the critical system and component parameters in an electro-optical imaging system, until a preliminary design that meets customer requirements is generated. An example of an eight band orbital imager was presented to demonstrate the methodology.

APPENDIX

A.1 Signal-to-Noise Based Figures-of-Merit

The signal and noise discussed in section 2.1.2. have units of photons $m^{-2}sec^{-1}$, or photon irradiance at a location just above the detector focal surface. Signal and noise can be referred to any point along the electro-optical system imaging chain. These alternative but equivalent descriptions are useful in the flowdown of requirements to the various subsystems in the imaging chain. This noise-equivalent representation refers to the aggregate effect of all of the imaging system stochastic noise sources (and these arise from different physical processes at different points along the image chain) to a particular convenient point in the imaging chain. A phenomenologist can quantitatively determine the minimum increase or decrease in the temperature, of a thermally radiating target which produces a signal change equal to the total imaging system noise. Likewise at the other end of the imaging signal chain, the electronics expert responsible for the specification of the system analog-to-digital converter (ADC), can determine the signal voltage range at the ADC input, corresponding to the total system noise. This allows proper sizing of the voltage range corresponding to the ADC's least-significant-bit (LSB).

In what follows both signal and noise-equivalent equations are given which establish the relationship between these quantities at key points along the imaging chain. We start by describing the propagation of signal information from the front to the back of the imaging chain. In addition, additive "non-signal" sources are traced through the imaging chain in order to facilitate proper sizing and analysis of the system dynamic range. The non-signal sources create offsets which reduce the dynamic range otherwise available for the signal. We assume that the electro-optical imaging system in question covers the spectral range from 0.4 to 12 μm. Nomenclature for the various spectral regions are defined in the table below.

Name	Acronym	Spectral Range
Visible	VIS	0.4 - 0.7 μm
Near Infrared	NIR	0.7 - 1.0 μm
Short-Wave Infrared	SWIR	1.0 - 2.5 μm
Mid-Wave Infrared	MWIR	2.5 - 7 μm
Long-Wave Infrared	LWIR	7 - 12 μm

For the VIS, NIR, and SWIR bands we assume that the scene contrast is produced by reflectance variations with spatial position within a scene, and for the MWIR and LWIR bands we assume that the scene contrast is provided by temperature and emissivity differences which vary with spatial position. The equations which follow describe the signal and associated noise-equivalent figures-of-merit (FOM's) for a single representative scene pixel. In what follows, signal associated with this representative scene pixel will be called "target" signal.

A.2 Signal Magnitude at different points in the Image Chain

For the VIS, NIR, and SWIR bands, the target (or ground) spectral radiance, defined at the location of a scene pixel is

$$L_s(\lambda) = \frac{\rho(\lambda)\, H_{s,exo}(\lambda) T_{atm}^{(d)}(\lambda)}{\pi} \qquad \text{(A1)}$$

$(W\ m^{-2} sr^{-1} \mu m^{-1})$

where $\rho(\lambda)$ is the target spectral reflectance which creates the scene contrast, $H_{s,exo}(\lambda)$ is the solar exo-atmospheric spectral irradiance, and $T_{atm}^{(d)}(\lambda)$ is the atmospheric spectral transmittance (downward). Note that $T_{atm}^{(d)}(\lambda)$ is a strong function of solar elevation angle; the source of illumination is the sun.

For the MW and LW "thermal" bands, the target spectral radiance is given by the Planck formula

$$L_s(\lambda) = \frac{\varepsilon(\lambda)\, 2hc^2}{\lambda^5 \left[\exp(hc/\lambda kT_{BB}) - 1\right]} \quad (A2)$$

$(W\ m^{-2}sr^{-1}\mu m^{-1})$

where $\varepsilon(\lambda)$ is the emissivity and T_{BB} is the temperature of a target scene pixel, λ is the wavelength, and h, c, k are Planck's constant, the speed-of-light, and Boltzmann's constant, respectively. The target radiances given by equations (A1) and (A2) are modified by upward transmission through the atmosphere to produce signal spectral radiance "at the top of the atmosphere" given by

$$L_s^{(top)} = T_{atm}^{(u)}(\lambda) L_s(\lambda) \quad (A3)$$

$(W\ m^{-2}sr^{-1}\mu m^{-1})$

where $T_{atm}^{(u)}(\lambda)$ is the atmospheric spectral transmittance (upward) and depends on the angle between the imaging system's light-of-sight and the normal to the target pixel surface. Nadir viewing implies that the sensor looks straight-down at the target pixels.

The target spectral radiance from a single scene pixel, modified by upward propagation through the atmosphere, produces a spectral irradiance at the sensor aperture given by

$$E_{AP}(\lambda) = \frac{L_s^{(top)}(\lambda)\,(TSD)^2}{R^2} \quad (A4)$$

$(W\ m^{-2}\mu m^{-1})$

where R is the target-to-image sensor range, and TSD is the target-sample-distance or linear dimension of the "footprint" of a focal plane detector pixel projected to the ground. The imaging equation gives

$$IFOV = \frac{TSD}{R} = \frac{x_d}{f_\ell} \quad (A5)$$

where IFOV is the instantaneous field-of-view of a pixel, x_d is the linear dimension of a pixel, and f_ℓ is the effective focal length. Equation (A4) is included because a related quantity, noise-equivalent aperture irradiance, is often used as a sensor-level FOM.

The imaging relationship given by equation (A5) allows us to express the target irradiance at a location just above the focal plane detector surface in terms of target spectral radiance. The equation for focal plane irradiance was given previously in section 2.1.1 [see equation (3)]. Since the purpose of this section is to discuss SNR-based FOM's, we simplify the analysis and notation by assuming that the discrete spectral bands of interest are quite narrow and approximated by $\Delta\lambda = \lambda_1 - \lambda_2$. This results in the simplification

$$\int_{\lambda 1}^{\lambda 2} a(\lambda)\, b(\lambda).....d\lambda \cong a(\bar{\lambda})\, b(\bar{\lambda}).....\Delta\lambda \qquad \text{(A6)}$$

where $a(\lambda)$, $b(\lambda)$, ..., are functions of λ, and $\bar{\lambda}$ is an "effective" wavelength defined at the center of the band or $\bar{\lambda} = (\lambda_2 + \lambda_1)/2$. With this simplification the focal plane irradiance is

$$\Phi_{S,FPA}(\bar{\lambda}) = E_{AP}(\bar{\lambda})\left[\frac{\pi D_0^2}{4}\right]\left[1 - \frac{D_{obs}^2}{D_0^2}\right]\left[\frac{T_o(\bar{\lambda})T_f(\bar{\lambda})\bar{\lambda}}{A_d\, hc}\right]\Delta\lambda \qquad \text{(A7)}$$

(photons m^{-2} sec^{-1})

where D_o is the optical aperture diameter, the factor $\pi D_o^2/4$ is the optical aperture area, D_{obs} is the diameter of the optical system's central obscuration, $T_o(\bar{\lambda})$ and $T_f(\bar{\lambda})$ are the optical train and spectral filter transmittances, respectively, the factor $hc/\bar{\lambda}$ is the energy of a photon of wavelength $\bar{\lambda}$, and $A_d = x_d^2$ is the area of a focal plane pixel. This later factor gives $\Phi_{s,FPA}(\bar{\lambda})$ in irradiance units of photons m^{-2} sec^{-1}.

Combining equations (A4), (A5), and (A7) we obtain

$$\Phi_{S,FPA}(\bar{\lambda}) = \left[1 - \frac{D_{obs}^2}{D_o^2}\right]\left[\frac{\pi}{4(f\#)^2}\right]\left[\frac{L_s^{(top)}(\bar{\lambda})T_0(\bar{\lambda})T_f(\bar{\lambda})\bar{\lambda}\Delta\lambda}{hc}\right] \qquad \text{(A8)}$$

(photons cm^{-2} sec^{-1})

where the focal ratio is $f\# = f_\ell/D_o$. Using the approximation in equation (A6) on our original definition of focal plane irradiance [equation (3), section 2.1.2], it is easy to show that we obtain a result identical to equation (A8) when we assume $\chi(\bar{\lambda}) \cong T_o(\bar{\lambda})T_f(\bar{\lambda})$. Equation (2), section 2.1.1 defines the radiance function $L_s(\lambda)$ at the top of the atmosphere.

The signal photon irradiance when absorbed by a detector pixel produces, a photocurrent equal to

$$I_S = q\Phi_{S,FPA}(\bar{\lambda})\eta_d(\bar{\lambda})A_d \qquad \text{(A9)}$$

(amps)

where q is the charge of an electron, and $\eta_d(\bar{\lambda})$ is the detector quantum efficiency at $\bar{\lambda}$. The number of photoelectrons generated during the integration time T_{int} is similarly,

$$N_S = \Phi_{S,FPA}(\bar{\lambda})\eta_d(\bar{\lambda})T_{int}A_d \qquad \text{(A10)}$$

(electrons)

The signal photoelectron charge, is actually integrated on a capacitive node typically in the unit cell readout circuit associated with each detector pixel. This integration produces a signal voltage

$$V_s = \frac{qG_{FPA}}{C_{int}} N_S \quad \text{(volts)} \tag{A11}$$

where G_{FPA} is the product of all the voltage gain factors from the unit cell capacitor to the focal plane output port. The integration capacitance is crucial to sizing the sensor signal dynamic range. A related useful quantity is the focal plane "conversion gain",

$$G_{conv} = \frac{qG_{FPA}}{C_{int}} \quad \text{(volts/electron)} \tag{A12}$$

Conversion gain values as high as 10 to 12 μvolts/electron are not uncommon in high-speed visible and infrared scanner designs aimed at moderate to low-light level applications.

The signal from the focal plane is then buffered, perhaps amplified, and delivered to a video ADC for digitization. The digital number corresponding to the signal level in equation (A11) is

$$DN_s = \frac{G_{sc} V_s}{\Delta V_{LSB}}, \quad \text{(unitless)} \tag{A13}$$

where ΔV_{LSB} is the voltage step corresponding to the least-significant-bit (LSB) of the ADC, and G_{SC} is the gain of the signal processing chain lying between the focal plane output and the ADC input. The quantity ΔV_{LSB} is given by

$$\Delta V_{LSB} = \frac{V_{ADC}}{2^n} \tag{A14}$$

where V_{ADC} and n are the ADC input voltage range and number of resolution bits, respectively.

The equations above [(A1) through (A14)] specify the propagation of signal information from the imaging chain input [i.e. radiance based on ground reflectance $\rho(\lambda)$ or ground temperature, T_{BB}] to the system output expressed as a digital number. In the next section we discuss imaging sensor dynamic range and maximum signal limitations using equations (A1) through (A14).

A.3. Signal saturation and dynamic range sizing

The maximum signal level that a sensor can accommodate is limited by the so-called "well capacity" or "well depth" of the focal plane pixels. This terminology derives from the saturation of a charge-coupled-device (CCD) pixel, based on the "charge-held-in-a-bucket" analogy for a CCD pixel. Most advanced multispectral sensors make use of hybrid infrared focal plane technology where the analog signal level is limited by the maximum charge which can be held by an integration capacitor with a fixed voltage across it. The maximum voltage permitted across this capacitor is limited by breakdown across capacitor's dielectric. The dielectric thickness and hence breakdown-limit is determined by the silicon CMOS readout fabrication technology. Clearly the absolute maximum signal limit is set by the input range of the ADC, or V_{ADC} in equation (A14). However, in most system designs, the limit is set by the maximum focal plane voltage swing and the factor G_{SC} is chosen to match this maximum FPA

swing to V_{ADC}. For the moment we ignore non-signal offset effects; their role in dynamic range sizing is treated later. Given this, it is instructive to define the focal plane irradiance, Φ_{FPA} using equations (A10) and (A11) as

$$\Phi_{s,FPA}(\bar{\lambda}) = \frac{V_s C_{int}}{G_{FPA} q \eta_d(\bar{\lambda}) T_{int} A_d} \tag{A15}$$

This equation makes explicit the factors which limit the maximum irradiance. Note that once $\Phi_{s,FPA}(\bar{\lambda})$ is known, equation (A8) determines the corresponding maximum signal radiance, and hence the maximum allowed reflectance for a given solar elevation angle (VIS, NIR, SWIR) or maximum target temperature (MW, LW) for a given target emissivity.

In equation (A15) the maximum FPA voltage, V_{ADC}, is limited by the readout integrated circuit technology. Since

$$\Phi_{s,FPA}(\bar{\lambda}) \propto \frac{C_{int}}{T_{int}}, \tag{A16}$$

the integration capacitance and integration time become the two key design parameters used to set the maximum signal level. For a scanning sensor, maximum system sensitivity occurs when T_{int} is set equal to T_{dwell}, the time it takes a pixel IFOV to scan its width or one TSD on the ground. It is possible in most modern focal plane designs to gate the integration time on command so that $T_{int}<T_{dwell}$; this is a powerful tool for managing dynamic range. This integration time gating also reduces in-scan pixel smear and increases the in-scan OTF. Decreasing T_{int}, however, reduces system sensitivity and SNR. The other key design parameter driven by maximum signal considerations is the integration capacitance, C_{int}. A desired $\Phi_{s,FPA}(\bar{\lambda})$ max, sets the value for C_{int} in the design. Having said this, it is important to note that both the maximum and minimum values of C_{int} can also be limited by practical design considerations.

The above discussion is only part of the story in dynamic range sizing. The system dynamic range must accommodate non-signal sources of radiance, detector dark current, focal plane/signal processing voltage offsets, and offset nonuniformities, in addition to the signal. These non-signal sources of radiance include those external to the sensor such as scattered, atmospheric thermal and path radiance, and those internal to the sensor such as straylight, and sensor thermal radiance along the optical imaging train.

The focal plane irradiances produced by these radiance sources are given by equations with the same functional form

$$\Phi_{ns,FPA}(\bar{\lambda}) = \frac{\Omega L_{ns}(\bar{\lambda}) T_{op}(\bar{\lambda}) T_f(\bar{\lambda}) \bar{\lambda} \Delta\lambda}{hc} \tag{A17}$$

(photons $m^{-2} sec^{-1}$)

where $L_{ns}(\bar{\lambda})$ is the spectral radiance of the non-signal source, and Ω is the effective solid angle which transforms this radiance source into a focal plane irradiance. The table below lists the appropriate forms for the parameters: Ω, $L_{ns}(\bar{\lambda})$ and $T_{op}(\bar{\lambda})$ to use in equation (A17) for each radiance source.

Source	$L_{ns}(\bar{\lambda})$ Non – Signal Source	Ω	$T_{op}(\bar{\lambda})$
External Radiance	External path, atmospheric scattered radiance	$\left[1-\frac{D_{obs}^2}{D_o^{\,2}}\right]\frac{\pi}{4(f\#)^2}$	$T_{op}(\bar{\lambda})$ of entire optical train
Optical Elements	$L_{ns}(\bar{\lambda}, \varepsilon_i, T_i)$ Planck formula for ith optical element	$\frac{\pi}{4(f\#)^2}$	Transmittance from ith optical element to focal surface
Cold Cavity	$L_{ns}(\bar{\lambda}, \varepsilon_{cc}, T_{cc})$ Planck formula for cold cavity inner surface	$\pi\left[1-\frac{1}{4(f\#)^2}\right]$	1.0 Focal surface directly exposed to inner surface of cold cavity

The total voltage offset at the focal plane output produced by all of these non-signal sources is

$$V_{off}^{(tot)} = V_{off}^{(radiance)} + V_{off}^{dark} + V_{off}^{(fp/sc)} + V_{off}^{(non-unif)} \quad \text{(volts)} \tag{A18}$$

where $V_{off}^{(radiance)}$ is the offset produced by the radiance sources, $V_{off}^{(dark)}$ is the offset produced by detector dark current, $V_{off}^{(non-unif)}$ is the voltage range spanning the detector offset non-uniformity, and $V_{off}^{(fp/sc)}$ is the offset produced by focal plane and signal chain electronics. Each of these terms is given below:

$$V_{off}^{(radiance)} = \sum_i \frac{\Phi_{ns,FPA}^{(i)}(\bar{\lambda}) G_{FPA} q \eta_d(\bar{\lambda}) T_{int} A_d}{C_{int}} \tag{A19}$$

which is obtained by combining equations (A10) and (A11) where the sum is over the i internal and external radiance sources with $\Phi_{ns,FPA}^{i}$ given by equation (A17), and;

$$V_{off}^{(dark)} = \frac{G_{FPA} T_{int} J_{dark} A_d}{C_{int}} \tag{A20}$$

which is obtained by combining equations (A9), (A10) and (A11), with $I_{dark} = J_{dark} A_d$ where I_{dark} is the dark current, and J_{dark} is the dark current/unit area. The detector dark current is a highly non-linear function of temperature and is inversely related to the detector internal impedance. The maximum voltage swing capability of the system, $V_s^{(max)'}$, must accommodate the sum of the maximum signal and all non-signal sources or,

$$V_s^{(max)'} = V_s^{(max)} + V_{off}^{(tot)} \tag{A21}$$

hence the maximum available signal voltage is

$$V_s^{(max)} = V_s^{(max)'} - V_{off}^{(tot)} \tag{A22}$$

where $V_{off}^{(tot)}$ is a function of C_{int}. Selection of C_{int} in the presence of these non-signal offsets therefore requires the use of equation (A22) rather than equation (A15). Of course these become equal when $V_{off}^{(tot)} \cong 0$. Minimizing $V_{off}^{(tot)}$ is a key goal in all imaging system designs. Reflecting the limit given by $V_{S,}^{(max)}$ to other points within the imaging chain is easily done by back substitution into equations (A10), (A9), (A8), (A4), (A3), (A2), and (A1).

A.4 Noise-Equivalent Measures

The signal equations described above can be used to reflect total system noise to any point along the imaging chain. Equations (A7), and (A8) do this at the focal plane surface in irradiance units. At this location we define noise-equivalent-irradiance (NEI) as the focal plane irradiance required to produce a signal-to-noise ratio of unity. The meaning of the various individual NEI terms is the same except that only the noise associated with that given term is used in the SNR=1 definition. To define these component NEIs, the noise associated with the particular component must be referenced to detector focal plane irradiance just as was done with the signal information in section 2.1.2. The root-sum-square (RSS) of all of the component NEIs then gives the total system NEI, per equation (6) of section 2.1.3. Note that implied in the very definition of NEI is the assumption that it represents one standard deviation of a random noise process which is well approximated by gaussian statistics.

We can readily obtain relationships between various system-level noise equivalent quantities by replacing $\Phi_{S,FPA}(\bar{\lambda})$ by $NEI(\bar{\lambda})$ in equations (A7), (A8), (A9), (A10), (A11), and (A13), and redefine each signal parameter by a noise-equivalent parameter. Starting at the digital back-end we replace DN_s by NEDN, then $\Phi_{S,FPA}(\bar{\lambda})$ by $NEI_{tot}(\bar{\lambda})$ to obtain

$$\underset{\text{(unitless)}}{NEDN} = \frac{G_{sc}G_{FPA}q\eta_d(\bar{\lambda})T_{int}A_d NEI_{tot}(\bar{\lambda})}{C_{int}\Delta V_{LSB}} \tag{A23}$$

where NEDN is the noise-equivalent digital number. Next we have

$$\underset{\text{(volts)}}{NEV} = \frac{G_{FPA}q\eta_d(\bar{\lambda})T_{int}A_d NEI_{tot}(\bar{\lambda})}{C_{int}} \tag{A24}$$

where NEV is the noise-equivalent signal voltage;

$$\underset{\text{(electrons)}}{NEE} = \eta_d(\bar{\lambda})T_{int}A_d NEI_{tot}(\bar{\lambda}) \tag{A25}$$

where NEE is the noise-equivalent number of electrons;

$$\text{NEPC} = q\eta_d(\bar{\lambda})A_d\text{NEI}_{tot}(\bar{\lambda}) \quad \text{(amps)} \tag{A26}$$

where NEPC is the noise-equivalent photocurrent;

$$\text{NEAI} \quad (\text{Wm}^{-2}\mu\text{m}^{-1}) = \frac{hc\,\text{NEI}_{tot}(\bar{\lambda})}{\left(\pi D_o^2/4\right)\left[1-\frac{D_{obs}^2}{D_0^2}\right]T_o(\bar{\lambda})T_f(\bar{\lambda})\bar{\lambda}\Delta\lambda} \tag{A27}$$

where NEAI is the noise-equivalent-aperture irradiance; and

$$\text{NESR}^{(top)} \quad (\text{Wm}^{-2}\text{sr}^{-1}\mu\text{m}^{-1}) = \frac{hc\,\text{NEI}_{tot}(\bar{\lambda})}{\left[1-\frac{D_{obs}^2}{D_0^2}\right]\left[\frac{\pi}{4(f\#)^2}\right]T_o(\bar{\lambda})T_f(\bar{\lambda})\bar{\lambda}\Delta\lambda} \tag{A28}$$

where $\text{NESR}^{(top)}$ is the noise-equivalent spectral radiance at the top of the atmosphere.

The noise-equivalent spectral radiance at the bottom of the atmosphere corresponding to equation (A3) is obtained by simply dividing the right-hand-side of equation (A27) by the upward atmospheric transmittance, $T_{atm}^{(u)}(\bar{\lambda})$.

Now that we have the $\text{NESR}(\bar{\lambda})$ defined in terms of NEI_{tot} at the source itself, we can define two additional noise-equivalent quantities related to the details of how the source radiance is produced. The two quantities are NEΔρ, the noise-equivalent reflectivity difference, and NEΔT, the noise-equivalent temperature difference. The quantity NEΔρ expressed in terms of NEI_{tot} is

$$\text{NE}\Delta\rho \quad (\text{unitless}) = \frac{4hc(f\#)^2\,\text{NEI}_{tot}(\bar{\lambda})}{H_{s,exo}(\bar{\lambda})T_{atm}^{(d)}(\bar{\lambda})\left[1-\frac{D_{obs}^2}{D_o^2}\right]T_o(\bar{\lambda})T_f(\bar{\lambda})\bar{\lambda}\Delta\lambda} \tag{A29}$$

where all of the symbols have been defined previously.

The quantity NEΔT is defined in terms of NEI_{tot} as

$$\text{NE}\Delta\text{T} \quad (\text{K}) = \frac{\text{NEI}_{tot}(\bar{\lambda})}{\left[\frac{\Delta\Phi_{s,FPA}(\bar{\lambda})}{\Delta T_{BB}}\right]} \tag{A30}$$

where the denominator represents the rate-of-change in observed focal plane irradiance with footprint temperature. Combining equations (A3) and (A8) we write

$$\frac{\Delta\Phi_{s,FPA}(\bar{\lambda})}{\Delta T_{BB}} = \left[1-\frac{D_{obs}^2}{D_o^2}\right]\frac{\pi T_o(\bar{\lambda})T_f(\bar{\lambda})\bar{\lambda}\Delta\lambda\Delta L_s(\bar{\lambda})}{4(f\#)^2\,hc\,\Delta T_{BB}} \tag{A31}$$

where using equation (A2) we calculate the thermal radiance temperature derivative

$$\frac{\Delta L_s(\bar{\lambda})}{\Delta T_{BB}} = \frac{dL_s(\bar{\lambda})}{dT_{BB}} = \frac{\varepsilon(\lambda)2h^2c^3\exp(hc/\lambda kT_{BB})}{\lambda^6 kT_{BB}^2\left[\exp(hc/\lambda kT_{BB})-1\right]} \qquad \text{(A32)}$$

$(W\ m^{-2}sr^{-1}\mu m^{-1}K^{-1})$

In analogy to the signal equations given in equations (A1) through (A13), the corresponding equations for the noise-equivalent FOM's are provided in equations (A23) through (A29), albeit in reverse order.

What remains to be done is define the equations for the various NEI components [equations (6) section 2.1.3] so that the NEI_{tot} can be computed. The NEI due to photon-noise has the general form

$$NEI = \sqrt{\frac{\Omega\, L(\bar{\lambda})T_{op}(\bar{\lambda})T_f(\bar{\lambda})\bar{\lambda}\Delta\lambda}{hc\,\eta_d(\bar{\lambda})T_{int}A_d}} \qquad \text{(A33)}$$

$(photons\ m^{-2}\ sec^{-1})$

which is identical to the formulas given in equations (7) through (12) of section 2.1.3 when the approximation given in equation (A6) is applied, an electronic bandwidth of $\Delta f = 1/2T_{int}$ is assumed and differences in definitions such as spectral exitance vs spectral radiance are accounted for. The NEI component due to dark current is

$$NEI_{dark} = \frac{\sqrt{J_{dark}A_d}}{\sqrt{qT_{int}\,\eta_d(\bar{\lambda})A_d}} \qquad \text{(A34)}$$

$(photons\ m^{-2}\ sec^{-1})$

where all of the symbols have been previously defined. The NEI component due to detector 1/f noise is

$$NEI_{1/f} = \frac{\sqrt{A\,\ell n\left[\frac{T_{recal}}{2T_{int}}\right]}}{q\,\eta_d(\bar{\lambda})\,A_d} \qquad \text{(A35)}$$

$(photons\ m^{-2}\ sec^{-1})$

where $\ell n \equiv$ natural logarithm, T_{recal} is the time between system offset recalibration and image data collection, and A is the detector current power-spectral-density evaluated at 1 Hz and has units of $amps^2/Hz$. The parameter A scales the magnitude of the detector 1/f-noise and depends strongly on detector temperature and detector bias.

Finally the NEI components due to voltage noise sources coming from anywhere in the system, but referenced to the focal plane output, is given by

$$NEI_{read} = \frac{C_{int}\,\sigma_v}{G_{FPA}\,q\,\eta_d T_{int}A_d} \qquad \text{(A36)}$$

$(photons\ m^{-2}\ sec^{-1})$

where σ_V is the rms voltage noise referenced to the detector output.

Equations (A33) to (A36) give the functional forms of all of the types of NEI components which arise in the computation NEI_{tot} as given by equation (6) in section 2.1.3.

A.5. Numerical example results for "LO" and "HI" radiance cases

The signal and noise-equivalent quantities discussed in this appendix were calculated using the imaging system design example outlined in section 3 of the paper. This was done for both the "LO" scene condition with results given in Tables I and II, and for the "HI" scene condition with results listed in Tables III and IV. Bands G and H require extremely large integration capacitors in order to limit the focal plane output swing to under 2 volts. This integration capacitance is most likely too large to be practical in a real focal plane design. Gating the integration time would be required resulting in additional loss of signal-to-noise ratio. The extremely large capacitor value combined with 300 μvolts of readout noise makes this the dominant noise source. Hence, in spite of the very large background levels in these bands, the sensor is readout-noise limited. One possible solution is to oversample the detector output during a dwell time, thus avoiding saturation. The sub-samples taken during the dwell time would then be added to synthesize the larger signal level. This would permit reduction of the integration capacitor size (improving noise) at the price of higher focal plane and ADC operating speeds and more complex processing.

The output parameters listed in tables II, III, IV, and V differ by 5 to 10 percent from equivalent parameters obtained in section 3. This is due to the rectangular filter approximation made via equation (A6) in order to simplify notation. In addition, bands G and H (as treated in this appendix) exhibit readout noise limited behavior due to the enormous integration capacitor sizes required to meet the dynamic range requirement within the focal plane voltage swing limit.

Table I. Multispectral Sensor Input Parameters

q	=	1.609×10^{-19} coul.	$f\#$	=	2
h	=	6.63×10^{-34} J.sec	T_{op}	=	0.75
c	=	3×10^{8} m/sec	T_f	=	0.75
k	=	1.38×10^{-23} J/K	η_d	=	0.75
$\varepsilon^{(LO)}$	=	0.8	G_{sc}	=	1.0
$T_{BB}^{(LO)}$	=	275 K	G_{FPA}	=	1.0
$\varepsilon^{(HI)}$	=	0.8	V_{ADC}	=	2 volts
$T_{BB}^{(HI)}$	=	375 K	n	=	12
$\rho^{(LO)}$	=	0.20	ΔV_{LSB}	=	488 μvolts
$\rho^{(HI)}$	=	0.80	$V_{FPA}^{(max)}$	=	2 volts
$\theta_{el,solar}^{(LO)}$	=	30°	J_{dark}	=	2 nA/cm^2
$\theta_{el,solar}^{(HI)}$	=	75°	σ_v	=	300 μvolts
R	=	500 km	T_{recal}	=	30 sec
D_o	=	0.3 m	A	=	10^{-28} amps^2/Hz at 1 Hz
D_{obs}	=	0.1 m	f_ℓ	=	0.6 m

Band	TSD (m)	X_d (μm)	T_{int} (msec)	$T_{ATM}^{(\omega)}$	C_{int}* (pf)	$(\bar{\lambda})$ (μm)	$\Delta\lambda$ (μm)
A	10.4	12.5	1.446	0.49	0.12	0.485	0.07
B	10.4	12.5	1.446	0.61	0.14	0.56	0.08
C	10.4	12.5	1.446	0.69	0.11	0.66	0.06
D	10.4	12.5	1.446	0.80	0.15	0.81	0.10
E	20.8	25	2.891	0.81	0.66	2.21	0.27
F	41.7	50	5.782	0.80	1.29	3.96	0.06
G	41.7	50	5.782	0.63	99.8	11.03	0.50
H	41.7	50	5.782	0.69	80.1	12.02	0.50

* C_{int} chosen to provide 20% margin on maximum FPA signal swing = 2.0 volts for "HI" radiance condition.

Table II. Signal Parameters : "LO" Signal Radiance

Band	ρ	T (K)	L_s $Wm^{-2}sr^{-1}\ \mu m^{-1}$	$L_s^{(top)}$ $Wm^{-2}sr^{-1}\ \mu m^{-1}$	$E_{AP}\ x10^{-8}$ $Wm^{-2}\ \mu m^{-1}$	$\Phi_{s,FPA}\ x10^{17}$ ph m^{-2} sec^{-1}	$I_s\ x10^{-11}$ (amps)	$N_s\ x10^5$ (electrons)	V_s (volts)	$DN_s^{(1)}$ (#)
A	0.2	-	57.1	28	1.2	4.67	0.88	0.79	0.106	216
B	0.2	-	49.2	30	1.3	6.62	1.24	1.12	0.129	264
C	0.2	-	42	29	1.25	5.65	1.06	0.96	0.143	293
D	0.2	-	27.5	22	0.952	8.77	1.64	1.49	0.161	331
E	0.2	-	2.7	2.2	0.381	6.47	4.85	8.8	0.212	435
F	-	275	1.3	1	0.696	1.17	3.52	1.27	0.157	322
G	-	275	12.7	8	5.56	218	654	236	0.378	776
H	-	275	10.2	6	4.17	178	535	193	0.386	790

Out of 4096 (1)

Table III. Noise-Equivalent Figures-of-Merit
"LO" Signal Radiance

Band	NEΔρ (%)	NEΔT (K)	NESR $Wm^{-2}sr^{-1}\ \mu m^{-1}$	$NESR^{(top)}$ $Wm^{-2}sr^{-1}\ \mu m^{-1}$	$NEAIx10^{-11}$ $Wm^{-2}\ \mu m^{-1}$	$NEI\ x10^{15}$ ph m^{-2} sec^{-1}	$NEPCx10^{-14}$ (amps)	N_{EE} (electrons)	$NEVx10^{-6}$ (volts)	NEDN
A	0.153	-	0.437	0.214	9.30	3.59	6.73	608	811	1.66
B	0.109	-	0.269	0.164	7.12	3.63	6.81	615	708	1.44
C	0.110	-	0.232	0.160	6.94	3.13	5.86	530	794	1.62
D	0.079	-	0.108	0.0866	3.76	3.46	6.49	586	638	1.37
E	0.038	-	0.0052	0.0042	0.725	1.23	9.22	1666	404	0.82
F	-	0.35	0.0030	0.0024	1.64	0.277	8.31	3002	370	.075
G	-	0.112	0.0101	0.0064	4.43	17.4	521	$1.89x10^5$	301	0.61
H	-	0.100	0.0080	0.0047	3.27	14.0	419	$1.51x10^5$	302	0.61

Table IV. Signal Parameters : "HI" Signal Radiance

Band	ρ	T (K)	L_s $Wm^{-2}sr^{-1}\,\mu m^{-1}$	$L_s^{(top)}$ $Wm^{-2}sr^{-1}\,\mu m^{-1}$	E_{AP} x10^{-7} $Wm^{-2}\,\mu m^{-1}$	$\Phi_{s,FPA}$ x10^{18} ph m^{-2} sec^{-1}	I_s x10^{-10} (amps)	N_s x10^6 (electrons)	V_s (volts)	$DN_s^{(1)}$ (#)
A	0.8	-	572	280	1.21	4.68	0.877	0.73	1.05	2164
B	0.8	-	459	280	1.21	6.17	1.16	1.05	1.20	2465
C	0.8	-	400	275	1.19	5.36	1.00	0.908	1.36	2788
D	0.8	-	250	200	0.865	7.97	1.49	1.35	1.47	3010
E	0.8	-	22.2	18	0.311	5.28	3.96	7.16	1.74	3555
F	-	375	13.8	11	0.765	1.29	3.88	14	1.73	3544
G	-	375	47.6	30	20.9	81.8	245	886	1.42	2910
H	-	375	33.9	20	13.9	59.4	178	644	1.286	2633

Out of 4096 (1)

Table V. Noise-Equivalent Figures-of-Merit
"HI" Signal Radiance

Band	NEΔρ (%)	NEΔT (K)	NESR $Wm^{-2}sr^{-1}\,\mu m^{-1}$	$NESR^{(top)}$ $Wm^{-2}sr^{-1}\,\mu m^{-1}$	NEAI x10^{-10} $Wm^{-2}\,\mu m^{-1}$	NEI x10^{15} ph m^{-2} sec^{-1}	NEPCx10^{-13} (amps)	N_{EE} (electrons)	NEVx10^{-6} (volts)	NEDN
A	0.122	-	0.871	0.427	1.86	7.16	1.34	1214	1618	3.31
B	0.099	-	0.572	0.349	1.52	7.73	1.45	1309	1507	3.08
C	0.101	-	0.503	0.347	1.51	6.79	1.27	1150	1725	3.53
D	0.079	-	0.2475	0.198	0.862	7.94	1.49	1345	1464	3.00
E	0.034	-	0.0094	0.0076	0.132	2.24	1.68	3036	736	1.51
F	-	0.029	0.0046	0.0037	0.254	0.428	1.28	4642	573	1.17
G	-	0.056	0.0101	0.0064	0.447	17.5	52.6	$1.89x10^5$	304	0.62
H	-	0.055	0.0080	0.0048	0.331	14.1	42.4	$1.51x10^3$	306	0.63

REFERENCES

[1] A. Papoulis, *Probability, Random Variables and Stochastic Processes*, McGraw-Hill, 1984.

[2] *The Infrared Electro-Optical Systems Handbook*, J. S. Accetta and D. L. Shumaker Eds., Information Analysis Center and SPIE Optical Engineering Press, Bellingham WA, Vol 1 - 8, 1993.

[3] G. C. Holst, *Electro-Optical Imaging System Performance*, JCD Publishing and SPIE Optical Engineering Press, Bellingham WA, 1995.

[4] G. Waldman, and J. Wooton, *Electro-Optical Systems Performance Modeling*, Artech House, 1993.

[5] T. S. Lomheim, and L. S. Kalman, "Analytical Modeling and Digital Simulation of Scanning Charge-Coupled Device Imaging Systems," *Electro-Optical Displays*, M. A. Karim Ed., Marcel Dekker Inc., pp 513-584, 1992.

[6] J. Vampola, *Readout Electronics For Infrared Sensors, The IR Electro-Optical Systems Handbook*, Vol. 3, SPIE Press, Bellingham WA, 1993.

[7] F. X. Kneizys et al., "Users Guide To LOWTRAN 7," AFGL-TR-88-0177, 1988.

[8] M. D. Nelson, J. F. Johnson, and T. S. Lomheim, "General Noise Processes in Hybrid Infrared Focal Plane Arrays," *Optical Engineering*, Vol. 30, no. 11, pp. 1682-1700, Nov. 1991.

[9] J. W. Goodman, *Introduction to Fourier Optics*, McGraw-Hill, 1968.

[10] R. G. Wilson, *Fourier Series and Optical Transform Techniques in Contemporary Optics*, John Wiley & Sons, 1995.

[11] T. S. Lomheim, and L. S. Kalman, "Analytical Modeling and Digital Simulation of Scanning Charge-Coupled Device Imaging System," *Electro-Optical Displays*, M. A. Karim Ed., Marcel Dekker, pp. 513-583, 1992.

[12] D. L. Fried, "Limiting Resolution Looking Down Through the Atmosphere," *Journal of the Optical Society of America*, Vol. 56, no. 10, pp. 1380-1384, Oct. 1966.

[13] F. Lei, and H. J. Tiziani, "Atmospheric Influence on Image Quality of Airborne Photographs," *Optical Engineering*, Vol. 32, no. 9, pp. 2271-2280, Sept. 1993.

[14] R. R. Beland, "Propagation Through Atmospheric Optical Turbulence," *Atmospheric Propagation of Radiation*, F. G. Smith Ed., Information Analysis Center and SPIE Optical Engineering Press, Bellingham WA, Vol. 2, pp. 157-232, 1993.

[15] E. L. O'neill, "Transfer Function for an Annular Aperture", *Journal of the Optical Society of America*, Vol. 46, no. 4, pp. 285-288, Apr. 1956.

[16] W. J. Smith, *Modern Optical Engineering*, McGraw-Hill, pp. 57-85, 1990.

[17] J. W. Goodman, *Statistical Optics*, John Wiley & Sons, pp. 374-384, 1985.

[18] Private Communication Perkin-Elmer.

[19] W. L. McCracken, "Infrared Line Scanning Systems," *Passive Electro-Optical Systems*, S. B. Campana Ed., Information Analysis Center and SPIE Optical Engineering Press, Bellingham WA, Vol. 5, p. 80, 1993.

[20] L. Schumann, and T. S. Lomheim, "Modulation Transfer Function and Quantum Efficiency at Long Wavelength in Linear Charge Coupled Imagers," *Applied Optics*, Vol. 28, no. 9, pp. 1701-1709, May 1989.

[21] J. F. Johnson, "Modeling Imager Deterministic and Statistical Modulation Transfer Functions," *Applied Optics*, Vol. 32, no. 32, pp. 6503-6513, Nov. 1993.

[22] D. H. Seib, "Carrier Diffusion of Modulation Transfer Function is Charge Coupled Imagers," *IEEE Trans. Electron Dev.*, Vol. 21, no. 3, pp. 210-216, March 1974.

[23] M. H. Crowell, and E. F. Labuda, "The Silicon Diode Array Camera Tube," *The Bell System Technical Journal*, pp. 1481-1528, May-June 1969.

[24] E. G. Stevens, "An Analytical, Aperture, and Two-Layer Carrier Diffusion MTF and Quantum Efficiency Model for Solid-State Image Sensor," *IEEE Trans. Electron Dev.*, Vol. 41, no. 10, pp. 1753-1760, October 1994.

[25] J. L. Harris, "Image Evaluation and Restoration," *Journal of the Optical Society of America*, Vol. 56, no. 5, pp. 569-574, May 1966.

[26] C. W. Barnes, "Object Restoration in a Diffraction-Limited Imaging System," *Journal of the Optical Society of America*, Vol. 56, no. 5, pp. 575-578, May 1966.

[27] A. V. Oppenheim, R. W. Schafer, *Digital Signal Processing*, Prentice-Hall, 1975.

[28] R. Barakat, "Application of the Sampling Theorem to Optical Diffraction Theory," *Journal of the Optical Society of America*, Vol. 54, no. 7, pp. 920-930, July 1964.

[29] J. L. Harris, "Diffraction and Resolving Power," *Journal of the Optical Society of America*, Vol. 54, no. 7, pp. 931-936, July 1964.

[30] F. O. Huck, N. Halyo, and S. K. Park, "Aliasing and Blurring in 2-D Imagery," *Applied Optics*, Vol. 9, no. 13, 2174-2181.

[31] E. A. Watson, R. A. Muse, and F. P. Blommel, "Aliasing and Blurring in Microscanned Imagery," *SPIE Infrared Imaging Systems*, Vol. 1689, pp. 242-250, 1992.